# Continuous Coherent Quantum Feedback with Time Delays: Tensor Network Solution

Kseniia Vodenkova and Hannes Pichler*

*Institute for Theoretical Physics, University of Innsbruck, 6020 Innsbruck, Austria*
*and Institute for Quantum Optics and Quantum Information of the Austrian Academy of Sciences, 6020 Innsbruck, Austria*

(Received 6 October 2023; revised 19 April 2024; accepted 10 July 2024; published 9 September 2024)

In this paper, we develop a novel method to solve problems involving quantum optical systems coupled to coherent quantum feedback loops featuring time delays. Our method is based on exact mappings of such non-Markovian problems to equivalent Markovian driven dissipative quantum many-body problems. In this work, we show that the resulting Markovian quantum many-body problems can be solved (numerically) exactly and efficiently using tensor network methods for a series of paradigmatic examples, consisting of driven quantum systems coupled to waveguides at several distant points. In particular, we show that our method allows solving problems in so far inaccessible regimes, including problems with arbitrary long time delays and arbitrary numbers of excitations in the delay lines. We obtain solutions for the full real-time dynamics as well as the steady state in all these regimes. Finally, motivated by our results, we develop a novel mean-field approach, which allows us to find the solution semianalytically, and we identify parameter regimes where this approximation is in excellent agreement with our tensor network results.

DOI: 10.1103/PhysRevX.14.031043 Subject Areas: Quantum Physics

## I. INTRODUCTION

Feedback is a cornerstone concept in modern technology, serving as the backbone for optimization and control in complex systems, where feedback loops take data from systems, process it, and adjust system parameters to achieve the desired outcome. Quantum feedback refers to the situation when the system of interest is quantum mechanical in nature [1–10]. Here, one can distinguish between two classes of feedback. In conventional, measurement-based quantum feedback, data are taken by projective or weak measurements, processed classically, and then used to adjust classical controls of the quantum system [1,2]. In contrast, *coherent* quantum feedback refers to the situation where the sensors, processors, and actuators are all quantum systems that interact coherently with the quantum system to be controlled [11,12]. In this scenario, the controller receives, processes, and feeds back quantum information [see Fig. 1(a)]. An exciting scientific frontier in this field is the exploration of phenomena that emerge in a regime when the controller can store and process the quantum state of multiple degrees of freedom.

In quantum optical systems, continuous coherent quantum feedback can be introduced naturally by reflecting the output radiation fields of a quantum emitter back onto the emitting system [13], e.g., by means of atom-photon interfaces in waveguide QED systems [14,15]. This kind of coherent feedback loops can acquire a true quantum many-body character when the associated *time delay* is large, i.e., when the time required for excitations to propagate through the feedback loop is large compared to the time required to emit an excitation, and the delay line can accommodate several excitations at a time [16]. Remarkably, several recent experiments across multiple platforms can now access this regime of large time delays. For instance, both in optical as well as in microwave settings, new milestones were established in scaling-up distances in distributed quantum networks [17–24]. Moreover, pioneering experiments with on-chip networks with superconducting devices also accessed this non-Markovian regime by employing slow excitation interconnects realized with structured waveguides [25,26] or by using propagating phononic modes [27–29].

On the theoretical side, dealing with time-delayed continuous coherent quantum feedback poses significant challenges, and traditional quantum optical techniques fail: Analytical treatments are limited to linear systems [30–32] or small excitation numbers in the feedback loops [33–40], while advanced, nonperturbative techniques [41–58] are typically limited to either finite time delays, or short-time dynamics. Among the latter, several approaches are based

*Contact author: hannes.pichler@uibk.ac.at

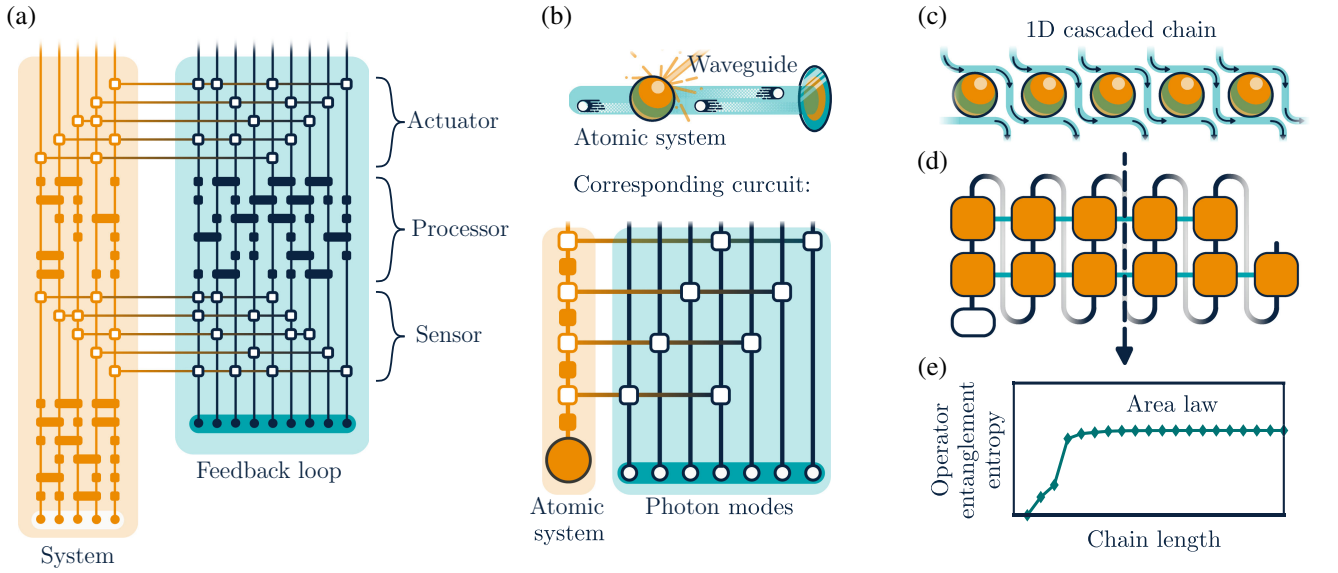


FIG. 1. Overview. (a) Schematic depiction of a generic coherent quantum feedback scheme, where a system interacts coherently with a feedback loop consisting of sensor, processor, and actuator. In this general illustration, both systems and feedback loop contain multiple degrees of freedom. (b) Simplest quantum optical setup that features continuous coherent quantum feedback, where photons propagating from an atomic emitter to a mirror and back represent the feedback loop. If the time delay in this process is large, the feedback loop can host multiple modes. The circuit representation of the dynamics (bottom) highlights the similarities with the generic scheme in (a). Note that in this setting the coherent feedback consists of only a sensor and a (delayed) actuator, since the processor acts trivially. (c) The problem in (b) can be exactly mapped to the Markovian problem of a 1D cascaded chain, where replicas of the atomic system interact with their nearest neighbors via cascaded channels. (d) The method developed in this work solves this problem by constructing a matrix product representation of the evolution operator of the 1D cascaded chain, together with a proper contraction scheme. Each block in (d) represents a tensor and connected lines indicate tensor contractions. (e) We find that the corresponding operator entanglement entropy obeys an area law; that is, the operator entanglement entropy of a subsystem does not increase with subsystem size. As a consequence, the maximum operator entanglement (over all subsystems) does not increase with the total systems size, as shown in (e). This underlies the efficiency of the method developed in this work.

on extending the Markovian cut and including the degrees of freedom of the feedback loop using tensor network techniques [41,43–45,51]. However, the computational cost associated with representing the feedback loop typically increases exponentially with the time delay [41]. A similar problem arises in approaches based on tensor network representation of the Feynman-Vernon influence functional [53–58], which are also expected to suffer from the growth of temporal entanglement with time delays. An alternative approach is based on representing the system dynamics in the form of a Markovian many-body system [42,52,59]. However, applications of this approach suffered from the exponential growth of the many-body Hilbert space, limiting the solution to short-time transient dynamics, preventing the access to steady-state quantities [60]. Predicting properties of systems subject to (continuous) coherent quantum feedback with time delays in generic parameter regimes, thus, remains an outstanding practical as well as conceptual challenge.

In this work, we address this challenge and develop methods for efficient and (numerically) exact solutions of the full real-time dynamics as well as the steady-state values of several important quantities of setups with continuous coherent time-delayed quantum feedback. Below, we first illustrate our method in detail on the simplest relevant example, that is, the problem of a single coherently driven two-level system coupled coherently to a long delay line shown in Fig. 1(b). Despite its simplicity, this problem already contains the essential challenges associated with coherent time-delayed quantum feedback and has, thus, served as a benchmark for numerical methods [41,42]. Based on this example, we review an exact relation between this non-Markovian problem and a corresponding Markovian many-body problem, the one-dimensional (1D) cascaded chain [42] [see Fig. 1(c)]. This relationship is established in two steps: We first represent the wave function of the quantum optical node and of the delay line as a 2D tensor network [16] and then relate the transfer operator of this tensor network to the propagator of the 1D cascaded chain. Our central technical result is that this propagator can be represented accurately and efficiently in matrix product form, and its operator entanglement entropy obeys an area law in the entire parameter space. Specifically, we show that the maximum operator entanglement entropy, which serves as a proxy for the computational cost associated with this representation, does

not increase with the chain length [see Fig. 1(d)]. Leveraging this insight allows us to solve for the real-time dynamics and the steady state of the reduced state of the system as well as for all low-order correlation functions of the propagating fields. We also show that analogous results hold for several additional, more complicated quantum optical problems with time delays, including the paradigmatic model of two driven, distant atoms coupled to a common waveguide, as well as multiatom generalizations thereof. Our work represents the first complete solutions of all these problems in their entire parameter regime and opens the door to study quantum optical phenomena in a so far inaccessible regime.

Finally, we also develop a semianalytical approach for the problems studied in this work. This is based on a mean-field approximation of the propagator of the 1D cascaded chain. This approach is motivated by our empirical observation that the effective bond dimension of the propagator is small in large regions of the parameter space. We show that our mean-field ansatz indeed reproduces the exact results in the relevant regions of parameter space.

## II. MODEL DESCRIPTION

### A. Continuous coherent quantum feedback with time delays

In this work, we develop a new approach to solving problems involving continuous coherent time-delayed quantum feedback. For the sake of clarity, we discuss this approach on the simplest but paradigmatic quantum optical model exhibiting time delays, consisting of a single driven nonlinear quantum optical system whose output is fed back to itself with a time delay. Physically, this is realized, e.g., by a driven atom coupled to a semi-infinite waveguide with a distant, perfectly reflecting mirror on one side, as shown in Fig. 2(a). The total Hamiltonian for this model consists of three terms describing the system (e.g., the atom), the bath (e.g., the waveguide), and their interaction, respectively:

$$H = H_{\mathrm{sys}} + H_B + H_{\mathrm{int}}. \tag{1}$$

For concreteness, below, we often use a two-level atom as an example representing the system, where the system Hamiltonian is given by

$$H_{\mathrm{sys}} = \hbar\omega_{eg}|e\rangle\langle e| - \frac{\hbar}{2}\left(\Omega|g\rangle\langle e|e^{\mathbb{i}\omega_0 t} + \mathrm{H.c.}\right) \tag{2}$$

Here, $\omega_0$ is a driving laser frequency, $\Omega$ is the Rabi frequency, $\omega_{eg}$ is the atomic transition frequency, and $\mathbb{i}$ is a complex unitary. We denote the states of the atom by $|g\rangle$ and $|e\rangle$ and the associated Hilbert space by $\mathcal{H}_{\mathrm{sys}}$. This model can be straightforwardly generalized to higher-dimensional systems, and we denote the system Hilbert space dimension by $d = \dim(\mathcal{H}_{\mathrm{sys}})$ in the following.

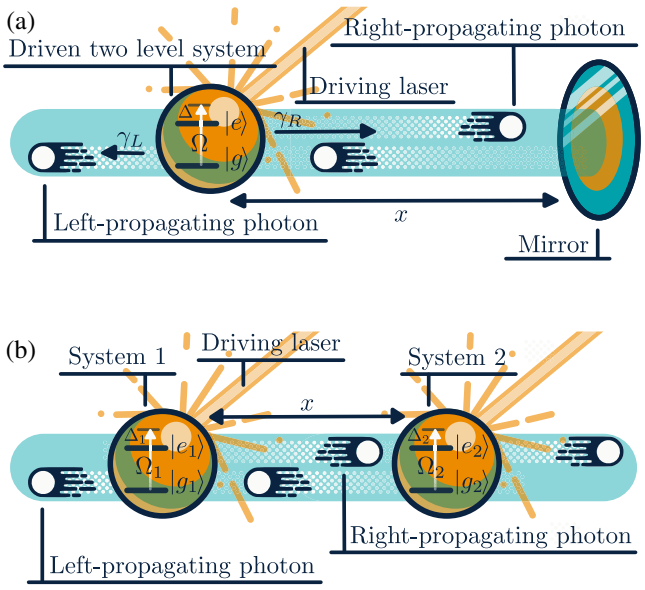


FIG. 2. Two schematic setups. (a) An atom in front of a mirror: A driven two-level system is coupled to a one-dimensional waveguide, terminated at one side by a mirror. (b) Two driven distant atoms coupled to a one-dimensional waveguide. In both setups, the systems are driven by a classical driving field, either via the waveguide or via a separate channel (as depicted here).

The bath Hamiltonian describing, e.g., a 1D semi-infinite waveguide is given by

$$H_B = \int d\omega\hbar\omega b^\dagger(\omega)b(\omega), \tag{3}$$

where $b(\omega)$ $[b^\dagger(\omega)]$ denotes a bosonic destruction (creation) operator of a bath excitation with frequency $\omega$. For convenience, we refer to these bath excitations as photons in the following. To describe the interaction of the system with the one-dimensional waveguide, we define system operators $c_L$ and $c_R$ associated with the coupling to the left- and right-propagating photons and corresponding decay rates $\gamma_L$ and $\gamma_R$. In general, these can be different for left- and right-moving photons, but for the simple two-level example we chose them to be the same; i.e., we use $c_L = c_R \equiv |g\rangle\langle e|$ and $\gamma_L = \gamma_R \equiv \Gamma/2$. The Hamiltonian representing the interaction between the system and the bath (in rotating wave approximation) is given by

$$H_{\mathrm{int}} = \frac{\mathbb{i}\hbar}{\sqrt{2\pi}}\int d\omega\Big[b^\dagger(\omega)\Big(c_L\sqrt{\gamma_L}e^{-\mathbb{i}\omega x/v} - c_R\sqrt{\gamma_R}e^{\mathbb{i}\omega x/v}\Big) - \mathrm{H.c.}\Big], \tag{4}$$

where $x$ denotes the distance between the atom and the mirror and $v$ the photon group velocity in the waveguide with linear dispersion relation. These are connected to the two quantities characterizing the delay line formed by the

reflecting waveguide: The delay time $\tau = 2x/v$ required by a photon to propagate from the atom to the mirror and back and the phase $\phi = \pi - \omega_0\tau$ that a photon with frequency $\omega_0$ accumulates during this round-trip. We note that couplings of the system to other Markovian environments can be included straightforwardly in this model.

We find it convenient to change from the frequency representation to a time representation of the waveguide radiation modes. For this, we introduce the so-called quantum noise operators

$$b(t) = -e^{-\mathrm{i}\omega_0\tau/2}\frac{1}{\sqrt{2\pi}}\int d\omega b(\omega)e^{-\mathrm{i}(\omega-\omega_0)(t-\tau/2)}, \quad (5)$$

which satisfy bosonic commutation relations $[b(t), b^\dagger(t')] = \delta(t-t')$. The operator $b^\dagger(t)$ creates a photon in the radiation mode labeled by $t$. The definition (5) differs from the conventional one [61] by a phase choice and a time shift, which simplifies notation in the following [62]. With this, the Hamiltonian Eq. (1) can be rewritten in the frame rotating with the laser frequency $\omega_0$ and in the interaction picture with respect to the bath Hamiltonian as

$$H^{R,I}(t) = H^{R,I}_{\mathrm{sys}} + H^{R,I}_{\mathrm{int}}(t). \quad (6)$$

In the example of the driven two-level system, we have $H^{R,I}_{\mathrm{sys}} = -\hbar\Delta|e\rangle\langle e| - \hbar/2(\Omega|g\rangle\langle e| + \mathrm{H.c.})$, with detuning $\Delta = \omega_0 - \omega_{eg}$. The interaction Hamiltonian takes the form

$$H^{R,I}_{\mathrm{int}}(t) = \mathrm{i}\hbar\Big([\sqrt{\gamma_R}b^\dagger(t+\tau)c_R + \sqrt{\gamma_L}b^\dagger(t)e^{\mathrm{i}\phi}c_L] - \mathrm{H.c.}\Big). \quad (7)$$

This formulation allows for a transparent interpretation of the dynamics: At each time instant $t$, the system interacts with two modes of the environment, namely, the ones labeled by $t+\tau$ and $t$. Note that the modes labeled $s$, with $t < s < t+\tau$, represent the field in the delay line at time $t$, i.e., the radiation field between the atom and the mirror. The modes that are located (at time $t$) to the left of the atom and propagate to the right are labeled with $s$, where $s > t+\tau$. The modes that are located (at time $t$) to the left of the atom and propagate to the left are labeled by $s$, with $s < t$ [cf. Fig. 2(a)]. As time progresses, the system thus interacts with each mode of the environment exactly twice. The time separation $\tau$ between these two events results in a memory of the environment that underlies the non-Markovian nature of this setup. While we derive the model described by Eq. (7) for the specific setup of an atom coupled to a semi-infinite waveguide, we note that it also applies to other setups, such as giant atoms [63] or collisional models [64].

### B. General quantum optical network

This example straightforwardly generalizes to an arbitrary network of $n$ distant quantum optical nodes interconnected by a set of $w$ photonic channels, which is described by a Hamiltonian of the form

$$H(t) = \sum_{i=1}^{n} H^{(i)}_{\mathrm{sys}} + \sum_{i=1}^{n}\sum_{j=1}^{w_i} H^{(i,j)}_{\mathrm{int}}(t), \quad (8)$$

where

$$H^x_{\mathrm{int}}(t) = \mathrm{i}\hbar\Big(\sqrt{\gamma_x}b^\dagger_{\sigma(x)}(t+\tau_x)c_x e^{\mathrm{i}\phi_x} - \mathrm{H.c.}\Big) \quad (9)$$

and $x = (i,j)$, a superindex. Here, a node $i$ is described by a system Hamiltonian $H^{(i)}_{\mathrm{sys}}$ and coupled to $w_i$ photon channels, with jump operators $c_{i,j}$ ($j \in \{1,\ldots w_i\}$). The $b_j(t)$ are quantum noise operators of the $j$th waveguides, satisfying $[b_j(t), b^\dagger_{j'}(t')] = \delta_{j,j'}\delta(t-t')$. The network structure is completely specified by a set of time delays $\tau_x$ and propagation phases $\phi_x$, as well as an index function $\sigma(x) \in \{1,\ldots w\}$. Here and in the following, we drop the superscript $R$, $I$ [cf. Eqs. (6)], since we always work in this frame from now on.

We note that this model includes the important example of two atoms coupled to a common 1D waveguide at two distant points; see Fig. 2(b). In this case, $w = 2$, corresponding to the left- ($\sigma = 1$) and the right- ($\sigma = 2$) moving modes in the waveguide. Moreover, we stress that the above models also describe so-called giant atoms that can potentially couple at multiple (distant) points to a waveguide [63]. Finally, we note that the above model can accommodate standard Markovian channels describing, e.g., the emission of photons into unguided modes. Such a general network can be used as a continuous quantum feedback setup, with some of the nodes playing the role of the feedback processor, allowing for more precise control.

## III. MAPPING TO 1D CASCADED CHAIN

In this section, we discuss how the physics of the non-Markovian problem of time-delayed coherent quantum feedback is related to the Markovian problem of the 1D cascaded chain [65]. This relationship forms the basis of our numerical algorithm described in Sec. IV. While we illustrate this relationship on the example defined in Sec. II A, the discussion directly generalizes to a subclass of quantum optical networks introduced in Sec. II B.

### A. Quantum state as 2D tensor network

#### 1. Quantum state of system and waveguide

We now integrate the Schrödinger equation associated with the Hamiltonian (6) for the total wave function of system and waveguide and introduce a convenient representation of this wave function using a tensor network. To start, we formally write the quantum state of the system and bath, i.e., the atom and radiation field, at time $t$ as

$|\Psi(t)\rangle = U(t-t_0)|\Psi(t_0)\rangle$, where the evolution operator is

$$U(t-t_0) = \mathcal{T}\left\{\exp\left(-\frac{i}{\hbar}\int_{t_0}^{t} H(t')dt'\right)\right\} \tag{10}$$

with $\mathcal{T}$ denoting time ordering. We consider for simplicity the initial state of the waveguide with all the modes in the vacuum state, i.e., $b(t)|\Psi(t_0)\rangle = 0$ for all $t \geq t_0$ [66]. A generalization to other important initial states of the waveguide (such as thermal, coherent, and squeezed states) is straightforward and discussed in Appendix B. To proceed, we find it convenient to discretize the total time of evolution in (infinitesimally) small steps $\Delta t$, such that $t_i = t_0 + i\Delta t$ and $\tau = k\Delta t$ with both $i$ and $k$ integer numbers. We define Ito increment operators for each time bin as $\Delta B_i = \int_{t_i}^{t_i+\Delta t} b(t')dt'$. They satisfy the bosonic commutation relations $[\Delta B_i, \Delta B_j^\dagger] = \Delta t\delta_{ij}$, such that we can associate a (bosonic) Hilbert space $\mathcal{H}_i$ with each time bin $i$ and denote its vacuum state by $|0_i\rangle$. Thus, we can Trotterize the evolution operator as $U(t_n - t_0) = U_{n-1}\ldots U_1 U_0$ with

$$U_i = \exp\left(-\frac{i}{\hbar}H_{\text{sys}}\Delta t + \Upsilon_i^L + \Upsilon_i^R\right), \tag{11}$$

where

$$\begin{aligned}\Upsilon_i^R &= \sqrt{\gamma_R}c_R\Delta B_{i+k}^\dagger - \text{H.c.},\\ \Upsilon_i^L &= \sqrt{\gamma_L}e^{i\phi}c_L\Delta B_i^\dagger - \text{H.c.}\end{aligned} \tag{12}$$

To simplify the following expressions, we introduce the notation $R = \sqrt{\gamma_R}c_R$ and $L = \sqrt{\gamma_L}e^{i\phi}c_L$. The unitary $U_i$ acts nontrivially only in the Hilbert space of the atom and the Hilbert space of time bins $i$ and $i+k$ (cf. Fig. 3). Since the waveguide is initially in the vacuum state, it is useful to form the isometry $V_i$: $\mathcal{H}_{\text{sys}} \otimes \mathcal{H}_i \to \mathcal{H}_{\text{sys}} \otimes \mathcal{H}_i \otimes \mathcal{H}_{i+k}$, which is induced by an application of the unitary map to the vacuum state of time bin $i+k$, $V_i = U_i|0_{i+k}\rangle$ [67]. With this, we can write the state at time $t_n$ as

$$|\Psi(t_n)\rangle = V_{n-1}\ldots V_1 V_0|\phi\rangle|v\rangle, \tag{13}$$

where $|\phi\rangle$ is the state of the system at time $t_0$ and $|v\rangle = \otimes_{i=0}^{k-1}|0_i\rangle$ is the initial state of the first $k$ time bins, i.e., the initial radiation field in the delay line. For the following discussion, we find it useful to depict Eq. (13) in the form of the tensor network shown in Fig. 3 (see Ref. [16] for a detailed discussion). Each isometry $V_i$ corresponds to a tensor in a two-dimensional square lattice. The size of the network along the first dimension (vertical direction in Fig. 3) is set by $k$, i.e., by the round-trip time $\tau$ in units of $\Delta t$, while the size along the second dimension (horizontal direction in Fig. 3) is given by $m = \lceil n/k \rceil$, i.e., total evolution time $t_n - t_0$ in units of the delay time $\tau$ rounded up. The bond dimension along the vertical direction, $\chi_v$, is set by the dimension of the system Hilbert space, $\chi_v = d$, while the bond dimension along the horizontal direction,

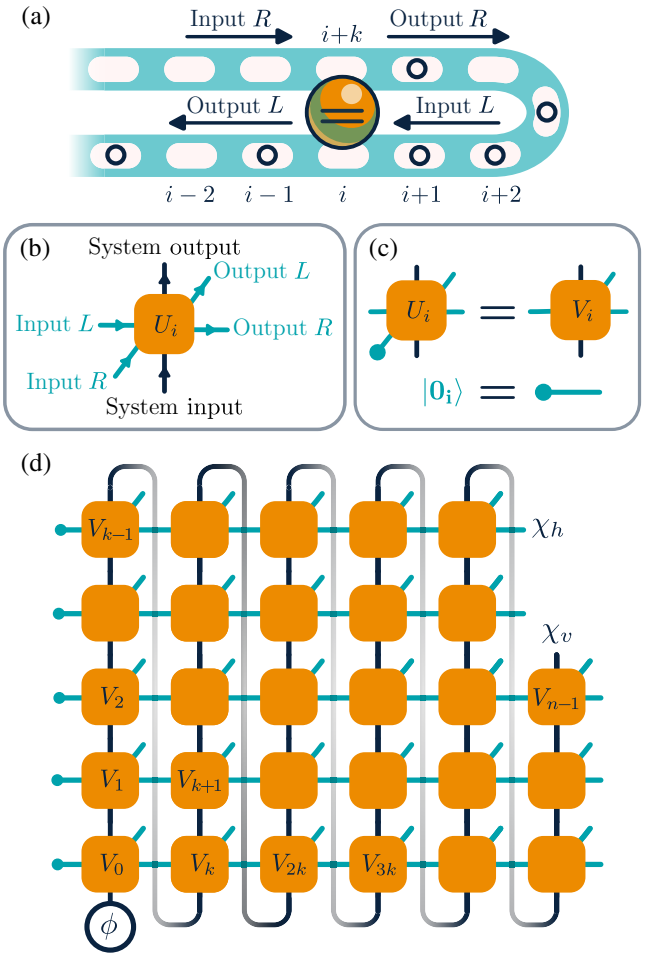


FIG. 3. (a) Illustration of the time discretization. The time bins represented by the white bubbles move as a conveyor belt in the directions pointed by the arrows, such that the system simultaneously interacts with the time bins $i$ and $i+k-1$. This interaction imposes a unitary map $U_i$ (b) acting on the atom and the two time bins. It is depicted here as a tensor with three input and three output legs ($L$ and $R$ stand for left- and right-moving time bins, respectively). Right-moving time bins assume to always have a vacuum input; therefore, we form an isometry $V_i$ (c). (d) Tensor network representing a total wave function of both the system and the waveguide at time $t_n$: The atom is initially in a state $\phi$, and the waveguide including the feedback loop is in a vacuum state. This tensor network corresponds to Eq. (13).

$\chi_h$, is set by the effective dimension of the bosonic modes associated to each time bin. For our workhorse example of the two-level system in front of the mirror, we have $\chi_v = \chi_h = 2$; that is, each time bin can host only zero or one photon. The reason for this lies in the fact that the probability to have more than one excitation $n_e$ in a single time bin is proportional to $(\Delta t)^{n_e}$ (see also Ref. [61]) and the error introduced by restricting the photon number vanishes in the limit $\Delta t \to 0$. An important peculiarity of the network geometry is the shifted periodic boundary conditions along the first dimension, as depicted in Fig. 3(d). We note that this state belongs to the class of

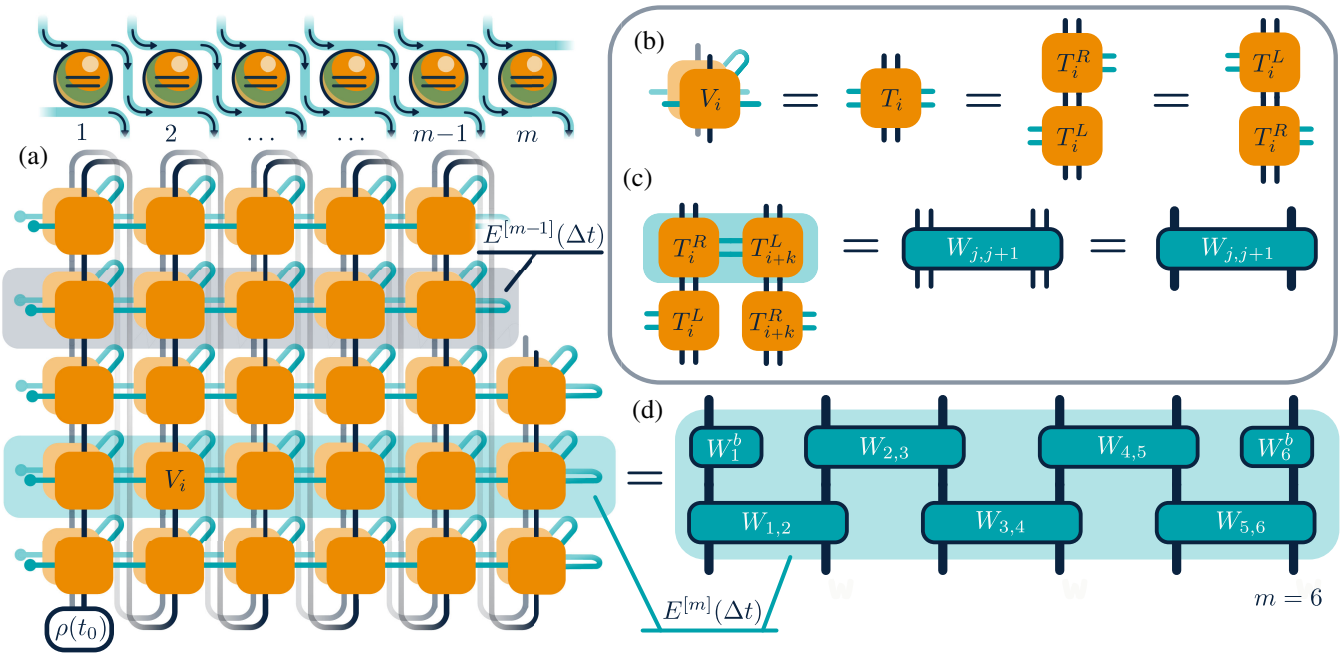


FIG. 4. (a) To obtain the reduced density operator of the atom, we "sandwich" the network of the wave function $|\Psi(t_n)\rangle$ (Fig. 3) with its counterpart $\langle\Psi(t_n)|$ and contract all the open legs containing photonic degrees of freedom (light blue legs) to trace out the bath. The transfer superoperator $E^{[m]}(\Delta t)$ for the resulting tensor network is indicated by the light blue area, while the dark blue area encloses $E^{[m-1]}(\Delta t)$. The superoperator $E^{[m]}(\Delta t)$ acts on $m$ replicas shown above the tensor network and consists of $m$ connected tensors $T_i$ (b) acting on the corresponding replica $\lceil i/k \rceil$. These tensors are decomposed as $T_i X = T_i^L T_i^R X$, corresponding to the right output field and the left input field. This decomposition is correct and symmetric up to higher-order Trotter terms: $T_i X = T_i^R T_i^L X$ [see Eq. (14)]. (c) The tensors acting on the adjacent replicas $T_i^R$ and $T_i^L$, when connected, form a two-site superoperator $W_{j,j+1} = \exp \mathcal{L}_{j,j+1}^{\text{casc}} \Delta t$ with $\mathcal{L}_{j,j+1}^{\text{casc}}$ defined by Eq. (17). For simplicity, we schematically represent double legs as one thick leg of dimension $d^2$. Tensors on the borders $T_1^L$ and $T_m^R$ do not have a connecting pair and result into one-site boundary local propagators $W_1^b = \exp \mathcal{L}_1^b \Delta t$ and $W_m^b = \exp \mathcal{L}_m^b \Delta t$ with the boundary terms defined by Eq. (18). With this, we show that the transfer operator $E^{[m]}(\Delta t)$ is an infinitesimal propagator for a 1D cascaded chain (d) as defined in Eq. (15).

2D isometric tensor network states [68–72], with its orthogonality center located in the lower left corner in Fig. 3. The isometric property of the tensors follows here directly from the sequential generation process.

#### 2. Reduced state of the system

One of the central quantities of interest is the state of the atom at time $t_n$, described by the reduced density operator $\rho_{\text{sys}}(t_n) = \text{tr}_{\mathcal{H}_B}\{|\Psi(t_n)\rangle\langle\Psi(t_n)|\}$. Here, the partial trace is performed over the Hilbert space of the radiation modes, $\mathcal{H}_B = \otimes_{i=0}^{n+k-1} \mathcal{H}_i$. For notational simplicity, we introduce a superoperator $T_i$, defined via $T_i X = \text{tr}_{\mathcal{H}_i}\{V_i X V_i^\dagger\}$. This allows us to write

$$\rho_{\text{sys}}(t_n) = \text{tr}_{\mathcal{H}_{\text{DL}}}\{T_{n-1} \ldots T_1 T_0 \Phi\}, \tag{14}$$

where $\mathcal{H}_{\text{DL}} = \otimes_{i=n}^{n+k-1} \mathcal{H}_i$ is the Hilbert space of the bosonic modes in the delay line (DL) and $\Phi$ denotes the projector onto the initial state $|\phi\rangle|v\rangle$. In tensor network notation, this expression takes on a simple form shown in Fig. 4: It corresponds to a contraction of a network of tensors on a square lattice with shifted periodic boundary conditions. Each tensor in this network corresponds to a map $T_i$, and its dimensions are given by $\chi_h^2$ and $\chi_v^2$ in the horizontal and vertical direction, respectively. As illustrated in Fig. 4, the tensor $T_i$ can be obtained from the tensors $V_i$ and $V_i^*$ by contracting the leg corresponding to the output field of the $i$th time bin.

### B. Relation to cascaded chain

To gain insight into the 2D tensor network defined by Eq. (14), it is useful to consider its transfer operator $E^{[m]}(\Delta t)$, as defined in Fig. 4. This transfer operator is a map from the $m$-fold replicated Hilbert space of system operators onto itself, i.e., $E^{[m]}(\Delta t) : \mathcal{B}(\mathcal{H}_{\text{sys}})^{\otimes m} \to \mathcal{B}(\mathcal{H}_{\text{sys}})^{\otimes m}$. Importantly, it can be shown that $E^{[m]}(\Delta t)$ can be exactly written as the (infinitesimal) propagator generated by a Lindblad superoperator $\mathcal{L}^{[m]}$, acting on these $m$ replica systems, that is,

$$E^{[m]}(\Delta t) = \exp\left(\Delta t \mathcal{L}^{[m]}\right). \tag{15}$$

Specifically, $\mathcal{L}^{[m]}$ is the Lindblad superoperator describing the dynamics of the *1D cascaded chain* of the $m$ replica systems described by the system Hamiltonian, such as in Eq. (2), i.e.,

$$\mathcal{L}^{[m]} = \mathcal{L}_1^b + \sum_{j=1}^{m-1} \mathcal{L}_{j,j+1}^{\mathrm{casc}} + \mathcal{L}_m^b. \tag{16}$$

Here, $\mathcal{L}_{j,j+1}^{\mathrm{casc}}$ is the Lindblad operator corresponding to a *cascaded coupling* between replicas $j$ and $j+1$. Such cascaded coupling has been studied by Gardiner and Carmichael [65,73] and, more recently, in the context of chiral quantum optical systems [74]. Cascaded couplings arise when an output field of a system (e.g., replica $j$) is injected as input to another system (e.g., replica $j+1$) via a unidirectional channel. In the 1D cascaded chain, nearest neighbors are coupled in this unidirectional manner (see Fig. 4 for an illustration). Mathematically, the Lindblad operator describing the cascaded interaction between replicas $j$ and $j+1$ is given by (cf. Ref. [61])

$$\mathcal{L}_{j,j+1}^{\mathrm{casc}} X = -\frac{\mathbb{i}}{\hbar}[H_{j,j+1}^{\mathrm{casc}}, X] + \mathcal{D}[R_j + L_{j+1}]X, \tag{17}$$

where we define the cascaded Hamiltonian

$$H_{j,j+1}^{\mathrm{casc}} = \frac{1}{2}\left(H_{\mathrm{sys},j} + H_{\mathrm{sys},j+1} + \mathbb{i}(R_j^\dagger L_{j+1} - L_{j+1}^\dagger R_j)\right)$$

and introduce the shorthand notation $\mathcal{D}[C]X = CXC^\dagger - \frac{1}{2}(C^\dagger CX + XC^\dagger C)$. Here, $H_{\mathrm{sys},j}$, $L_j$, and $R_j$ are simply the system Hamiltonian [e.g., Eq. (2)] and jump operators, acting on the $j$th replica system. Note that the total Lindblad operator (16) also contains the boundary terms, which are simply given by

$$\begin{aligned}\mathcal{L}_1^{\mathrm{bd}L} X &= -\frac{\mathbb{i}}{2\hbar}[H_{\mathrm{sys},1}, X] + \mathcal{D}[L_1]X,\\ \mathcal{L}_m^{\mathrm{bd}R} X &= -\frac{\mathbb{i}}{2\hbar}[H_{\mathrm{sys},m}, X] + \mathcal{D}[R_m]X,\end{aligned} \tag{18}$$

and act independently only on the first and the last replica. We refer the reader to Fig. 4 for a diagrammatic derivation of this equivalence between the transfer operator $E^{[m]}(\Delta t)$ and the propagator of the 1D cascaded chain. A formal derivation can be found in Appendix A. This correspondence has an intuitive physical origin already pointed out in Ref. [42]: The right-propagating output field emitted by the system at a time $s$ becomes the left-propagating input field of the system at a later time $s+\tau$. In turn, the right-propagating output field of the system at time $s+\tau$ turns into the left-propagating input field of the system at time $s+2\tau$, etc. The different replicas in the cascaded chain, thus, assume a role analogous to the one of the system at different points in time, separated by multiples of $\tau$. From this equivalence between the tensor network transfer operator and the infinitesimal propagator of the 1D cascaded chain, it is straightforward to see that the reduced state of the system, $\rho_{\mathrm{sys}}(t_n)$, can be obtained from the finite-time propagators $E^{[m]}(s) = \exp\left(s\mathcal{L}^{[m]}\right)$. To be specific, we define $r$ via $t_n = (m-1)\tau + r$, with $0 \le r \le \tau$. As shown in Fig. 4(a), the reduced state of the system, $\rho_{\mathrm{sys}}(t_n)$, can be obtained from contracting $E^{[m]}(r)$ with $E^{[m-1]}(\tau - r)$, with shifted periodic boundary conditions, and applying the resulting composite map to the initial state of the system, $\rho_{\mathrm{sys}}(t_0)$. Denoting the contraction imposed by shifted periodic boundary conditions applied to a tensor network $X$ by $\mathcal{P}(X)$, we can write

$$\rho_{\mathrm{sys}}(t_n) = \mathcal{P}\left(E^{[m-1]}(\tau - r)E^{[m]}(r)\right)\rho_{\mathrm{sys}}(t_0). \tag{19}$$

This contraction can be conveniently performed if $E^{[m]}(s)$ is given in matrix product form, as discussed in the next section.

### C. Multinode networks

The mapping of the delayed quantum feedback problem to the 1D cascaded chain described above can be generalized to more complicated networks with multiple nodes. Below, we present, for simplicity, the results for certain networks where all time delays between nodes are identical. In Appendix D 2, we generalize the results to the situation of nonequal time delays and more complicated networks. The reduced state of the multiple nodes is always described by a 2D tensor network (with generalized shifted periodic boundary conditions), whose transfer operator is the propagator of a 1D unidirectional master equation on several replicas of the nodes (with potentially long-range interactions). An important example in this class is the problem of two distant nodes, $A$ and $B$, interacting with a common, bidirectional waveguide, where the time delay due to the photon propagation between the two nodes in both directions is identical: For large time delays, the node dynamics is non-Markovian, but again it maps to the Markovian problem of a 1D cascaded chain with a two-site unit cell where every odd site corresponds to a replica of node $A$ and every even site to a replica of node $B$. We refer the reader to Appendix D 1 for a detailed derivation of this correspondence.

## IV. NUMERICAL METHODS

### A. Matrix product form of the propagator

We are aiming now to efficiently represent the propagator of the 1D cascaded chain, $E^{[m]}(s) = \exp\left(s\mathcal{L}^{[m]}\right)$ for $0 \le s \le \tau$, using matrix product state (MPS) techniques. For this, we first recall that $E^{[m]}(s)$ is a linear operator which maps the Liouville space of $m$-fold replicated system operators, $\mathcal{B}(\mathcal{H}_{\mathrm{sys}})^{\otimes m}$, onto itself. Following the literature

(e.g., Ref. [61]), we refer to such maps as superoperators. Note that such superoperators form a $d^{4m}$-dimensional vector space. Defining $D = d^4$, this vector space is the tensor product space of $m$ $D$-dimensional vector spaces, each a local superoperator vector space $\mathcal{C}$, whose elements act only on one site of the 1D chain and map $\mathcal{B}(\mathcal{H}_{\text{sys}})$ onto itself. The tensor product space is, therefore, $\mathcal{C}_m = \mathcal{C}^{\otimes m}$. We choose a basis of $\mathcal{C}$ and denote its basis elements by $S_i$, with $i = 1, \ldots, D$, from which we can construct a product basis of $\mathcal{C}_m$. With this, we can write any superoperator $\mathcal{S} \in \mathcal{C}_m$ in a matrix product form:

$$\mathcal{S} = \sum_{j_1, j_2, \ldots, j_m = 1}^{D} C_{j_1}^{[1]} C_{j_2}^{[2]} \cdots C_{j_m}^{[m]} S_{j_1} \otimes S_{j_2} \otimes \cdots \otimes S_{j_m}, \tag{20}$$

where $S_{j_i}$ is a local basis superoperator on the site $i$ and the summation includes all such superoperators. The matrix $C_{j_i}^{[i]}$ associated with the local basis superoperator $S_{j_i}$ has dimension $\chi \times \chi$, with $\chi \geq 1$ being the bond dimension of $\mathcal{S}$ (the boundary tensors $C_{j_1}^{[1]}$ and $C_{j_m}^{[m]}$ are simply vectors of length $\chi$). We refer to a superoperator in the above form as matrix product superoperator (MPSO).

### 1. Evolution equation

To construct a representation of the finite-time propagator $E^{[m]}(s)$ in the matrix product form Eq. (20), we first recall that it satisfies

$$\frac{d}{ds} E^{[m]}(s) = \mathcal{L}^{[m]} E^{[m]}(s), \tag{21}$$

with the initial condition $E^{[m]}(0) = \mathbb{1}^{\otimes m}$. Importantly, $E^{[m]}(0)$ is a product (super)operator. Moreover, $\mathcal{L}^{[m]}$ contains only nearest-neighbor terms. Therefore, we can use the standard time-evolving block decimation (TEBD) algorithm [75] to integrate Eq. (21). For this, we Trotterize the propagation with the cascaded Lindbladian for an infinitesimal time step into $m-1$ nearest-neighbor propagators, $W_{j,j+1} = \exp(\Delta t \mathcal{L}^{\text{casc}}_{j,j+1})$, and two local boundary terms $W_1^b = \exp(\Delta t \mathcal{L}_1^b)$ and $W_m^b = \exp(\Delta t \mathcal{L}_m^b)$ [see Figs. 4(d) and 5(a)]. The computational cost of the associated updates in the matrix product representation for each such two-site update is $O(\chi^3 d^{12})$. Note that the time step $\Delta t$ in this Trotterization has to be chosen much smaller than the timescale on which the system evolves, e.g., $\Delta t \ll 1/|\Omega|, 1/|\Delta|, 1/\Gamma$. In all our numerical results below, we check convergence in the size of $\Delta t$.

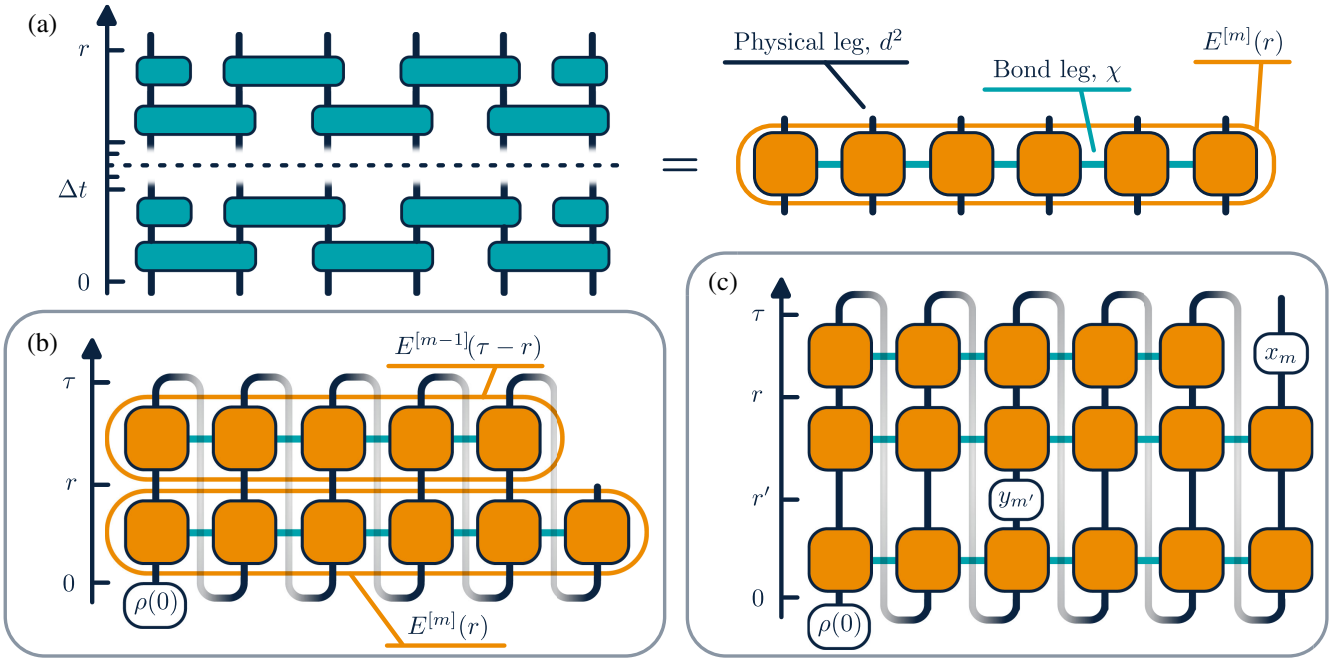


FIG. 5. Tensor network illustration of the numerical method described in Sec. IV. (a) The propagator $E^{[m]}(r)$ is obtained by the Trotterized evolution of $m$ sites until time $r$ [see Eq. (21)]. (b) The reduced density matrix of the atom $\rho_{\text{sys}}(t_n)$ is a result of contraction of the propagators $E^{[m]}(r)$ and $E^{[m-1]}(\tau - r)$ [see Eq. (19)]. (c) The two-times correlation function of the system operators $\langle x(t) y(t') \rangle$ requires a contraction of the three propagators with the system operators inserted between them at the corresponding times and sites as indicated in Sec. IV A 3 [Eqs. (22) and (23)].

#### 2. System density operator

Once the propagators $E^{[m]}(s)$ are obtained in matrix product form, the reduced state of the system can be calculated at all times $t \leq m\tau$ via Eq. (19). For this, first note that one can obtain $E^{[m-1]}(s)$ directly from $E(m,s)$: Because of the unidirectional nature of a cascaded chain, one can simply trace out the $m$th replica to obtain the propagator for a shorter chain, that is, $E^{[m-1]}(t) = (1/d)\mathrm{tr}_m\big(E^{[m]}(t)\big)$. The contraction (19) can then be performed efficiently, since it can be cast in the form of a 1D tensor network contraction as shown in Fig. 5(b). The computational cost of this contraction is $O(m\chi^3 d^4)$.

#### 3. Multitime correlation functions

Beside the system density operator, we are also interested in the properties of the radiation field. Importantly, arbitrary field correlation functions can be related to multitime correlation functions of system operators, using input-output relations (see Ref. [61]). Multitime correlation functions can be accessed by a straightforward generalization of the above discussion. For instance, consider the two-times correlation function $\langle x(t)y(t')\rangle$ for two arbitrary system operators $x$ and $y$. We introduce the notation $\langle\cdots\rangle = \langle\Psi(t_0)|\ldots|\Psi(t_0)\rangle$ for quantum mechanical expectation values and denote the system operator $x$ in the Heisenberg picture at time $t$ by $x(t) = U^\dagger(t-t_0)xU(t-t_0)$. Without loss of generality, we consider $t > t'$. We define integers $m$ and $m'$ as well as remainders $r$ and $r'$, via $t = (m-1)\tau + r$ and $t' = (m'-1)\tau + r'$. We then can write $\langle x(t)y(t')\rangle = \mathrm{tr}(\mathcal{P}(M)\rho(0))$ with

$$M = E^{[m-1]}(\tau - r)x_m E^{[m]}(r - r')y_{m'}E^{[m]}(r') \quad (22)$$

for $r \geq r'$ and

$$M = E^{[m-1]}(\tau - r')y_{m'}E^{[m]}(r' - r)x_m E^{[m]}(r) \quad (23)$$

for $r < r'$. Here, $x_m$ denotes the operator $x$, acting on the $m$th replica, and $y_{m'}$ is defined analogously [see Fig. 5(c)]. Again, this contraction can be performed efficiently with a cost given by $O(m\chi^4 d^4)$. This can be straightforwardly generalized to arbitrary $p$-times correlation functions of system operators. It is easy to see that the corresponding contraction can be performed at a cost $O(m\chi^{p+2}d^4)$, leading to an exponential scaling with the order of the correlation function $p$.

### B. Infinite cascaded chain

One of the most important quantities of interest is the steady state of the system density operator, $\rho_{\mathrm{ss}} = \lim_{t\to\infty}\rho(t) = \lim_{m\to\infty}\rho(m\tau)$. If the steady state is unique, it can be expressed in terms of the finite-time propagator of an infinite 1D cascaded chain [see Eq. (19)] as

$$\rho_{\mathrm{ss}} = \lim_{m\to\infty}\mathcal{P}\Big(E^{[m]}(\tau)\Big)\frac{\mathbb{1}}{d}. \quad (24)$$

Importantly, we can directly target the steady state of the system by directly calculating infinite system size propagator using infinite matrix product state techniques [76]. For this, one assumes a translation invariant matrix product representation of $E^{[\infty]}(s)$, with $C^{[k]}(s) = C(s)$ (for all $k$) and integrates Eq. (21) self-consistently from $s = 0$ to $s = \tau$ [77]. Besides accessing $\rho_{\mathrm{ss}}$, this enables the calculation of multitime system correlation functions in the steady state using expressions analogous to Eqs. (22) and (23) and, in turn, field correlation functions via input-output relations. Moreover, one can also directly access the relaxation time $t_{\mathrm{ss}}$ of the system: This is determined by the correlation length $\xi$ of $E^{[\infty]}(\tau)$, via $t_{\mathrm{ss}} = \xi\tau$. Since $E^{[\infty]}$ is given in translational invariant matrix product form, its correlation length can be directly accessed from spectral decomposition of the tensor $C^{[k]}(\tau)$. For details regarding the infinite chain algorithm, we refer the reader to Appendix C.

### C. Multinode networks

As discussed in Sec. III C, we consider $n$-node networks where all time delays are identical. These can also be mapped to 1D cascaded chains. Therefore, we can straightforwardly generalize the numerical methods introduced above to such multinetwork setups. Figure 6 illustrates this generalization for setups with two and three atoms. In each case, the tensor network representing the reduced state of the $n$ nodes can be constructed from the propagator of a 1D cascaded chain with an $n$-site unit cell. Specifically, as shown in Figs. 6(b) and 6(c), the state of the nodes is obtained from a contraction of $n$ such propagators with $n$-fold shifted periodic boundary conditions. For each 1D cascaded chain, we construct this propagator using standard TEBD procedure in the exact same way as for the case of a single node. The computational cost of constructing the propagator is independent of the number of nodes $n$. However, the cost of contraction scales as $O(m\chi^{3+2(n-1)}d^{4+2(n-1)})$, where $n$ is the number of the nodes in the model, and we assume that all nodes have the same local Hilbert space dimension $d$.

## V. RESULTS

### A. Propagator bond dimension

We now proceed to discuss the computational cost of the method outlined in the previous section, i.e., the cost of constructing the propagator of the 1D cascaded chain. The computational cost depends crucially on the bond dimension of $E^{[m]}(\tau)$: The problem of interest can be solved efficiently if the matrix product representation of $E^{[m]}(\tau)$ obeys an area law for all $\tau$, that is, if the bond dimension $\chi$ required to represent the $E^{[m]}(\tau)$ grows at most polynomially with $m$. Important quantities in this context are the singular values of the splitting of $E^{[m]}(\tau)$ in two partitions formed by the first $\ell$ replicas and the last $m-\ell$ replicas,

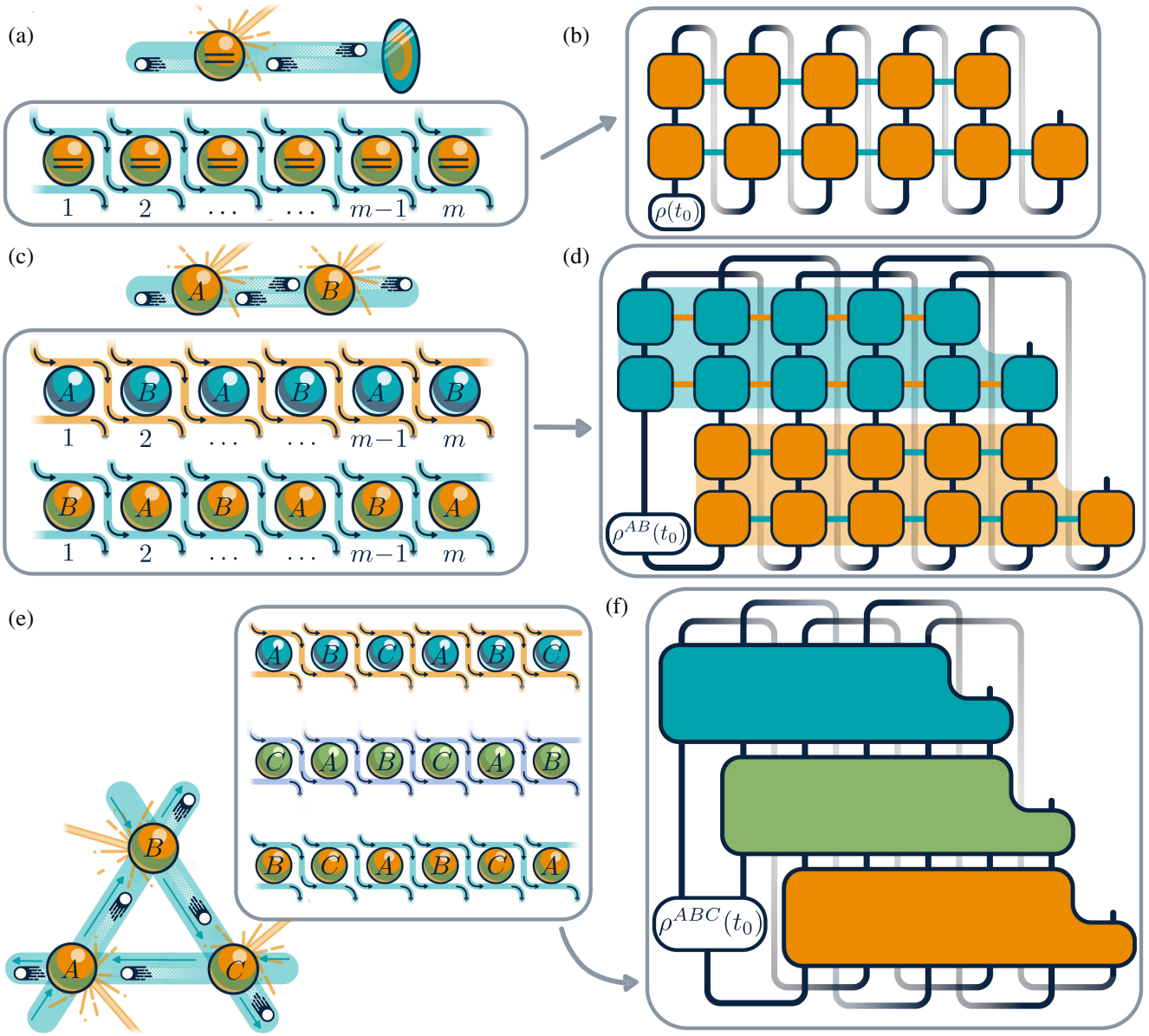


FIG. 6. Generalization of our approach to the multinode networks discussed in Sec. IV C. (a) The atom in front of the mirror is mapped to 1D cascaded chain of identical replicas corresponding to the state of the atom at a different time. The chain is evolved using MPS methods to obtain the total propagator, which is then contracted (b) with the shifted periodic boundary conditions and applied to the initial density operator. (c) A problem of the setup with two atoms connected through a bidirectional waveguide is mapped to two cascaded chains. (d) The propagators obtained after the evolution of these chains are then contracted together with the double-shifted periodic boundary conditions. (e) A configuration with three atoms connected through a unidirectional waveguide is mapped to three cascaded chains. (f) The resulting three propagators are contracted with the triple-shifted periodic boundary conditions.

respectively. We denote these singular values by $\sigma_\alpha$ (with $\alpha = 1, \ldots, \chi$) and define normalized singular values as $\bar{\sigma}_\alpha = \sigma_\alpha / (\sum_\beta \sigma_\beta^2)^{1/2}$. We also introduce the entropy of the normalized singular values associated with this splitting:

$$S(\ell) = -\sum_\alpha \bar{\sigma}_\alpha^2 \log_2(\bar{\sigma}_\alpha^2), \tag{25}$$

as well as the maximum entropy among all cuts of the chain $S = \max_\ell S(\ell)$, and use it as a proxy for the bipartite correlations in the propagator and the effective bond dimension $\chi \sim 2^S$. One can distinguish two qualitatively different behaviors of $S(\ell)$ for large $\ell$: If $S(\ell)$ grows (linearly) with $\ell$, one calls this a *volume law* (since $\ell$ is the subsystem volume); if $S(\ell)$ saturates to a constant value, one calls this an *area law* (since the subsystem boundary in 1D is independent of the subsystem size). An area law of the entanglement entropy implies that $S$ also saturates to a constant value as the chain length $m$ grows, as $S(l)$ becomes independent of the subsystem size. The entropy

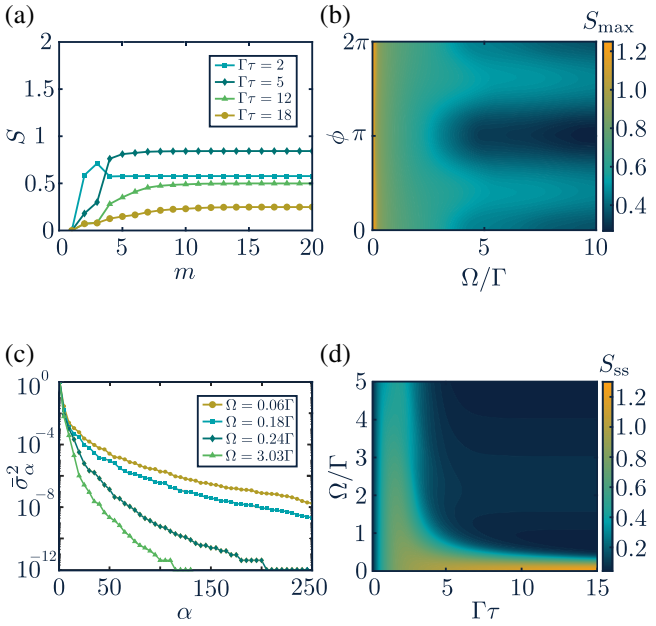


FIG. 7. Entropy area law demonstrated for the propagator of the atom in front of the mirror. (a) Dependence of the bipartite entropy $S$ on the length of the chain $m$ exhibiting an area law for $\Gamma\tau = 2,\ 5,\ 12,\ 18$ and $\Omega/\Gamma = 0.5$, $\chi = 50$, and Trotter step $\Gamma\Delta t = 0.05$. (b) The dependence of the maximum entropy during the time evolution, $S_{\max} = \max_\tau S$, on the phase and the Rabi frequency for $m = 20$, $\chi = 80$, and $\Gamma\Delta t = 0.05$. (c) Steady-state normalized singular values squared corresponding to the maximum entropy bipartition for different driving strengths, $\Gamma\tau = 20$, $\phi = 0$, $\chi = 250$, and $\Gamma\Delta t = 0.1$. (d) Steady-state entropy $S_{\rm ss}$ for different delay times $\Gamma\tau$ and Rabi frequencies, $\phi = \pi$, $\chi = 100$, and $\Gamma\Delta t = 0.001$. For all plots, the detuning $\Delta/\Gamma = 0$.

area law implies that the operator can be represented efficiently as MPO for an arbitrary number of sites in the chain, since the corresponding bond dimension is independent of the system size $\chi \sim 2^S$, where $S$ is the saturation entropy value.

In Fig. 7(a), we show $S$ as a function of $m$ for the 1D cascaded chain corresponding to our example of a driven two-level atom coupled to a delay line (see Sec. II A). Importantly, this shows a clear area law for all values of $\tau$; that is, the entropy saturates to a finite value as $m$ increases. We calculate the saturation entropy value also for different round-trip phases and driving strengths in Fig. 7(b), where we plot the maximum value of the entropy in the nonzero delay time range, $S_{\max} = \max_\tau S$. To give a more detailed perspective on the (operator) entanglement properties, we show in Fig. 7(c) the squared normalized singular values in the steady state for different driving strengths. This indicates once again the efficiency of the matrix product representation of the propagator, since one can truncate the bond dimension $\chi$ in a controlled way and reach sufficiently small truncating errors even for bond dimensions $\chi \ll \chi_{\max} \sim d^m$. In Fig. 7(d), we show the entropy saturation value, calculated for an infinite number of replicas, and confirm that the saturation value is finite in the entire parameter space. Perhaps counterintuitively, the saturation value is the highest for zero driving, despite the existence of an analytical solution in that case (for a single excitation). This is resolved by noting that the operator entropy is calculated for the propagator of the cascaded chain and, therefore, contains information about the dynamics of all possible initial states of the cascaded chain, including those where multiple excitations are present. More importantly, the entropy is remarkably small if both $\tau$ and $\Omega$ are large, demonstrating the applicability of our method even in previously inaccessible regimes, that is, efficient calculation of a transient dynamics for an unlimited number of round-trips in the case of both long delay times and multiple excitations in the delay line. We use this feature in Sec. VII and propose a semianalytical approach to describe the system in this latter regime. While our results in Fig. 7 demonstrate the area law explicitly for the 1D cascaded chain of driven two-level systems, we find analogous results also for other examples (see Appendix D). In general, one expects an area law for the propagator of a 1D Markovian master equation whenever it is rapidly mixing; i.e., its mixing time scales at most logarithmic with $m$ [78].

We note that the entanglement entropy area law and, therefore, efficient classical calculation of the state of the system do not contradict the results of Ref. [16], where it was shown that universal resource states for measurement-based quantum computing can be generated from a single emitter with time-delayed feedback. In order to harness the cluster state as a resource for quantum computation, one needs to measure every (relevant) mode of the output field. This is indeed equivalent to calculating a very high order correlation function. In contrast, our method allows us to efficiently access few-body observables, such as the reduced state of the emitter(s), or few-body correlations functions of the output field.

## B. Single driven atom in front of a distant mirror

### 1. Atomic dynamics and steady state

In this subsection, we present results obtained from solving for the dynamics and the steady state of the atom in front of the mirror, using the methods developed in the previous sections.

In Fig. 8(a), we plot the evolution of the atomic excitation probability for a resonant driving field as a function of time, $\rho_{ee}(t) = \langle e|\rho(t)|e\rangle$, for up to 15 round-trip times with long time delays $\Gamma\tau = 20$ and a round-trip phase of $\phi = \pi$. To interpret the results, it is useful to recall that a two-level atom in its ground state acts like a mirror for photons in a frequency band of width $\Gamma$ around the two-level transition frequency. With the choice of $\phi = \pi$, the delay line and the atom, therefore, form a perfect cavity for a (single) photon that is resonant with the atomic transition frequency. This effect leads to a dynamical accumulation of

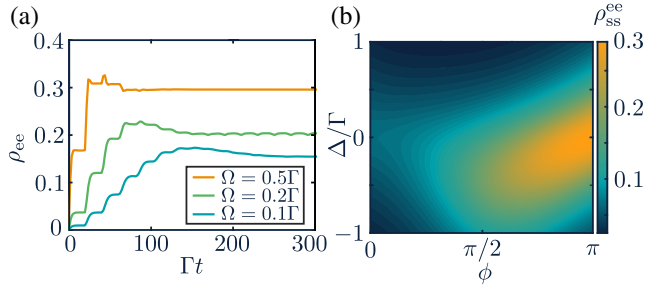


FIG. 8. Excited state probability of the atom in front of the mirror. (a) Probability dynamics for the various driving strengths $\Omega = 0.1, 0.2, 0.5\Gamma$, delay time $\Gamma\tau = 20$, $\phi = \pi$, $\chi = 80$, and $\Delta/\Gamma = 0$. (b) Excited state probability in the steady state as a function of the round-trip phase $\phi$ and the detuning $\Delta/\Gamma$, $\Omega/\Gamma = 0.5$, $\Gamma\tau = 20$, and $\chi = 50$. The Trotter step is $\Gamma\Delta t = 0.1$ for both plots.

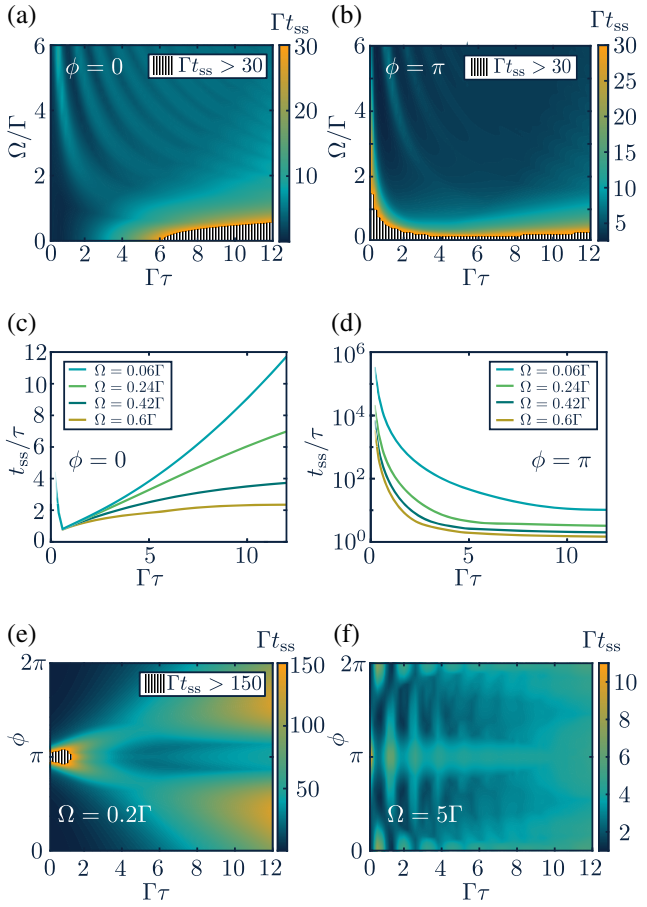


FIG. 9. Steady-state time $t_{ss}$ of the atom in front of the mirror. (a),(b) The dependence on Rabi frequencies and delay times, $\phi = 0$, and $\phi = \pi$. (c),(d) The steady-state time relative to the delay time in the small driving limit for different values of $\Omega$, $\phi = 0$, and $\phi = \pi$. (e),(f) The steady-state time calculated for the different phases and delay times, $\Omega = 0.2\Gamma$, and $\Omega = 5\Gamma$. For all plots, the parameters are $\Gamma\Delta t = 0.1$, $\chi = 250$, and $\Delta/\Gamma = 0$.

photons in the delay line, as long as the atomic excitation probability is small. This dynamic proceeds until the field in the delay line is strong enough to effectively saturate the two-level atom, rendering it nonreflective and allowing photons to leak out of the delay line. This interplay between photon trapping and atom saturation determines the steady state. If the coherent driving field is very weak, it takes several round-trip times until this point is reached, while for a stronger drive the atom saturates much quicker due to the coherent drive.

If the coherent driving field is not resonant with the two-level system transition frequency, i.e., if the detuning $\Delta$ is nonzero, the reflectivity of the atom and, thus, the trapping capabilities of the setup change. In fact, these trapping capabilities are determined by a nontrivial interplay between the detuning and the round-trip phase. This is displayed in Fig. 8(b), where we show the steady-state excitation probability of the atom, which is related to the photon number in the delay line via the input-output relation. In Fig. 8(b), we show only half of the round-trip phase range, since the excitation probability has a symmetry $\Delta \to -\Delta$ and $\phi \to -\phi$. This symmetry already appears in the case of an atom with (instantaneous) coherent feedback [41]. Specifically, one can define the effective detuning $\Delta_{\text{eff}} = \Delta - \gamma/2\sin(\phi)$ with the last term indicating the so-called phase-dependent Lamb shift. This detuning is invariant under simultaneous sign change of $\Delta$ and $\phi$. To give further intuition into the qualitative features in Fig. 8(b), we note that the structure of the plot can be understood by analyzing the analytic solution for zero driving field [79]. One can show that in the absence of a driving field a nontrivial dark steady state exists if $|\mathbb{i}\Delta - \gamma(1 + e^{-\mathbb{i}\phi})| = 0$. Signatures of this dark state survive also for finite driving so that the steady-state excitation probability is enhanced around the dark state condition.

As noted, our method allows us also to directly access the time it takes the system to relax to its steady state, $t_{ss}$. Figure 9 shows $t_{ss}$ for a resonant drive as a function of delay time and driving strength as well as round-trip phase. Because of the photon-trapping mechanism discussed earlier, we observe long relaxation times in the regime of weak driving and long delay times; for large enough Rabi frequencies, $t_{ss}$ oscillates with a period proportional to $2\pi/\Omega$. This can be understood by noting that the Rabi oscillations of the atom affect the probability of the photon to be reflected by the atom. When the delay time becomes large enough for the atom to reach an equilibrium state during a round-trip time, these oscillations damp out. The round-trip phase also affects the chances of a photon to be trapped, thus increasing the steady-state time as seen in Fig. 9(b).

### 2. Output field properties

The infinite chain algorithm for the atom in front of the mirror discussed earlier can be used to calculate the steady-state properties of the output field, such as the spectrum and the intensity correlation functions.

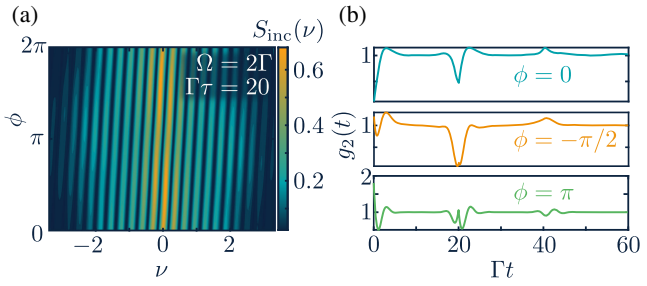


FIG. 10. Steady-state output field properties for the setup with the atom in front of the mirror. (a) The dependence of the incoherent part of the spectrum $S_{\mathrm{inc}}(\nu)$ on the round-trip phase. (b) The dependence of the second-order correlation function $g_2(t)$ on the delay time $\Gamma\tau$ for the round-trip phases $\phi = 0, \pi/2, \pi$; for both plots, $\Omega = 2\Gamma, \Gamma\tau = 20, \Delta/\Gamma = 0, \chi = 80$, and $\Gamma\Delta t = 0.01$.

The steady-state spectrum of the output field detected at the open side of the waveguide is given by

$$S(\nu) = 2\mathrm{Re}\left\{\int_0^\infty dt' \left\langle b_{\mathrm{out}}^\dagger(t) b_{\mathrm{out}}(t-t')\right\rangle e^{-i\nu t'}\right\}, \quad (26)$$

where the output field operator is obtained using the input-output formalism as

$$b_{\mathrm{out}}(t) = \sqrt{\gamma_L} c_L(t) + \sqrt{\gamma_R} e^{-i\phi} c_R(t-\tau) + e^{-i\phi} b(t), \quad (27)$$

where we use the definition $b_{\mathrm{out}}(t) = e^{i\omega_0\tau/2}\frac{1}{\sqrt{2\pi}} \times \int d\omega b(\omega, t' > t) e^{-i(\omega-\omega_0)(t-\tau/2)}$ with $b(\omega, t')$ being a bosonic operator in the Heisenberg picture. Based on the expression Eq. (27), the output spectrum can be obtained from two-times system correlation functions (see Appendix C for details). The incoherent part of the spectrum in the case of the long delay time and for different round-trip phases is shown in Fig. 10(a) and exhibits a pattern of minima and maxima with a periodicity proportional to $1/\tau$. This periodicity is a result of the correlations between the photons emitted with the time difference $\tau$. Using the input-output formalism Eq. (27), one can also calculate the normalized second-order correlation functions of the output field:

$$g_2(t') = \frac{\left\langle b_{\mathrm{out}}^\dagger(t) b_{\mathrm{out}}^\dagger(t-t') b_{\mathrm{out}}(t-t') b_{\mathrm{out}}(t)\right\rangle}{\left\langle b_{\mathrm{out}}^\dagger(t) b_{\mathrm{out}}(t)\right\rangle \left\langle b_{\mathrm{out}}^\dagger(t-t') b_{\mathrm{out}}(t-t')\right\rangle}. \quad (28)$$

The result is shown in Fig. 10(b) for different round-trip phases and exhibits both bunching and antibunching behavior depending on the round-trip phase. This behavior occurs due to the fact that the output field consists of both the field that is directly emitted by the atom into the output port and the field that first passes through the delay line and only then leaves through the output port. Generically, one expects both these fields to be each independently anti-bunched, since they are emitted by a two-level system.

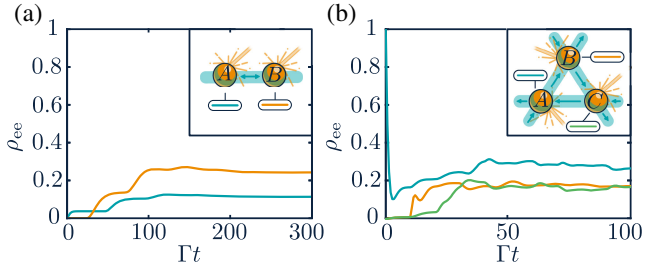


FIG. 11. Excited state probabilities dynamics for the multinode setups. (a) $\rho_{\mathrm{ee}}^A$ and $\rho_{\mathrm{ee}}^B$ of the two atoms $A$ and $B$ connected through the bidirectional waveguide as a function of $\Gamma t$. Both atoms are initially in the ground state, with parameters $\gamma_1 = \Gamma/2$, $\gamma_2 = \Gamma/10$, $\Omega_1 = \Gamma/5$, $\Omega_2 = 0$, $\phi = \pi$, $\Gamma\tau = 20$, and $\chi = 50$. (b) The excited state probabilities $\rho_{\mathrm{ee}}^A$, $\rho_{\mathrm{ee}}^B$, and $\rho_{\mathrm{ee}}^C$ of the three atoms $A$, $B$, and $C$ connected through 1D unidirectional waveguides as a function of $\Gamma t$; initially, the atoms are in the excited, ground and ground states; $\gamma_1 = \gamma_2 = \gamma_3 = \Gamma/2$, $\Omega_1 = \Gamma/2$, $\Omega_2 = \Omega_3 = \Gamma/10$, $\phi = \pi$, $\Gamma\tau = 10$, and $\chi = 25$. For both plots, $\Delta/\Gamma = 0$ for all nodes and $\Delta t = 0.1$.

Bunching can, however, occur, when a first photon is emitted into the delay line and upon its return triggers a stimulated emission of a second photon from the atom into the output port, leading to two photons in the output. For this effect to happen, several factors need to align. First, the delay line needs to be long enough, such that the atom can get reexcited before the first photon completes its round-trip. Thus, this effect is exclusively present in the non-Markovian limit. Second, the round-trip phase needs to be chosen to avoid destructive interference for the stimulated emission process, which explains the differences in the plots for various round-trip phases.

### C. Other networks

In this subsection, we present results from the application of our method to other simple quantum optical networks, connecting two or three nodes. Figure 11(a) shows the dynamics of a pair of two-level atoms coupled to a bidirectional waveguide at two distant points. The time delay is a result of the propagation time a photon needs to travel between the two systems. For this case, we assume $\gamma_{i,R} = \gamma_{i,L} = \gamma_i$ and $\Gamma = 2\gamma_1$. Next, Fig. 11(b) shows the dynamics of three nodes connected pairwise with unidirectional waveguides, with equal time delay in each interconnect. Here, again, $\gamma_{i,R} = \gamma_{i,L} = \gamma_i$ and $\Gamma = 2\gamma_1$. These results can be obtained through an adaptation of the derivation given in Sec. III B and a corresponding, simple modification of the algorithm given in Sec. IV. We discuss these generalizations to more complicated networks in detail in Appendix D.

## VI. COMPARISON WITH EXISTING METHODS

In this section, we analyze the cost and limitations of the method presented in this paper and compare it with existing

TABLE I. Comparison of computational cost for various numerical methods for the problem of a single node with time-delayed coherent quantum feedback studied in this work (see the text for definitions).

| Method | Time evolution | Steady-state access | Density matrix | Two-times correlation functions |
|---|---|---|---|---|
| Ref. [41] | $O(nk\chi^3 d^3)$, $\chi \sim 2^{\gamma\tau}$ | Indirect, finite $\tau$ | $O(\chi d)$ | $O(k\chi^3 d)$ |
| Ref. [42] | $O(d^{6m})$ | No | $O(d^{2(m+1)})$ | $O(d^{2(m+1)})$ |
| This work | $O(mk\chi^3 d^{12})$, $\chi \sim$ const | Direct | $O(m\chi^3 d^4)$ | $O(m\chi^4 d^4)$ or $O(m\chi^3 d^4)$ [80] |

methods. Specifically, we compare it with two methods that have been recently developed and which have been applied to several problems.

The first is a method proposed in Ref. [41]. The central idea underlying that approach is to represent the wave function of the entire system containing node(s) as well as waveguide(s) using a 1D MPS. The Hilbert space of the bosonic modes in this approach is also decomposed in time-bin modes, which are organized in a 1D array according to their time label. This matrix product state is then propagated using the Hamiltonian Eq. (7), e.g., using the TEBD algorithm, which allows one to access real-time evolution. In this 1D construction, time delays lead to long-range interactions, which, in turn, result in long-range entanglement and correspondingly require a large bond dimension $\chi$ of the MPS, scaling typically exponentially with the time delay. Accessing systems with very long time delays is, thus, prohibitively expensive with that approach. For instance, for the paradigmatic problem of a single atom in front of a mirror, the regime $\gamma\tau \gtrsim 10$ is out of reach for state-of-the-art implementations of this approach. In contrast, the method presented in this work does not encounter this exponential barrier and allows one to access the long-time-delay regime with polynomial costs [see Figs. 7, 8(a), 10, and 11(a) in Sec. V].

Another approach to solve problems with time-delayed feedback was given in Ref. [42], which is based on solving for the propagator of the cascaded chain using exact numerics. This is an exact method that does not suffer from long time delays. Instead, it is limited to finite evolution times. More specifically, the exact dimension of the replica-operator space grows exponentially with the number of round-trip times as $d^{4m}$, and exact diagonalization of the cascaded propagator within this space scales exponentially with the number of round-trips. Correspondingly, exact numerics are accessible only for problems with very small dimension of the node Hilbert space and for the transient dynamics up to few round-trip times. This limit is overcome by the method introduced in this paper, where computational cost grows only polynomially with the number of the round-trips and the steady state can be targeted directly (see Figs. 7–10 in Sec. V).

In Table I, we list the costs of certain procedures of each method mentioned above. In the first column, we compare the cost of evolution, that is, the cost of evolving the total wave function in the method proposed in Ref. [41] and the cost of calculating the cascaded propagator performing exact diagonalization in the method presented in Ref. [42] as well as in the method presented in this paper. We recall here that the delay time is given as $\tau = k\Delta t$, a total evolution time $t_n = n\Delta t$, $m = \lceil n/k \rceil$, and $d$ is a local Hilbert space dimension of the system. The second column indicates whether the method under consideration provides access to the steady state of the system (atom). The third column shows the computational cost of contraction required to obtain the system density matrix after the evolution is performed. For the method in Ref. [41], one has to contract the total wave function in MPS form. The algorithm presented in Ref. [42] requires a contraction of $d^{2m} \times d^{2m}$ matrix of the cascaded propagator. As discussed before, in this work, we contract the cascaded propagator in MPS form, which leads to a favorable scaling. Last, we also compare the cost of calculating the two-times correlation functions. For the method in Ref. [41], this leads to a contraction of the total MPS wave function with the operators applied to the sites separated by at most $k-1$ sites. The method from Ref. [42] requires one to perform another propagator evolution at a cost $O(d^{6m})$ with the operators inserted during the evolution followed by a contraction, the cost of which is the same as for the density matrix calculation. Our method offers two ways of computing two-times correlation functions. That is, one can use the results of the propagator evolution obtained before, insert operators, and then contract with the cost of contraction being $O(m\chi^4 d^4)$, or one can again perform the evolution with the operators inserted on the way and then contract MPSO at a cost $O(m\chi^3 d^4)$.

In addition to this qualitative analysis of the scaling behavior, we also perform a quantitative comparison of the run-time of different algorithms on the same problem. The results are presented in Appendix E.

As discussed above, the main advantage of our method lies in the fact that it does not scale exponentially with time delay or with evolution time. We note, though, that the scaling with the dimension of the local Hilbert space $d$ is less favorable when compared to Ref. [41]; see Table I. This limits the applicability in settings with large-node Hilbert spaces. In particular, in setups where the nodes themselves are composed of many-body systems, the cost of a direct application of this (as well as other) method(s) becomes prohibitively expensive. In such scenarios, one can attempt to combine the tools developed here with efficient state

representations of the node Hilbert space. A simple example of such an extension is presented as part of the following section.

## VII. MEAN-FIELD APPROXIMATION

In this section, we use the insights of the numerical results from Sec. V to propose a semianalytical solution based on the mean-field approximation of the 1D cascaded chain. As Fig. 7 indicates, the correlations in the propagator $E^{[m]}(s)$ are small when both the time delay and the Rabi frequency are large [81]. This suggests that in this regime the $m$-site propagator $E^{[m]}(s)$ can be approximated as a tensor (direct) product of local propagators:

$$E^{[m]}(s) \approx \bigotimes_{j=1}^{m} E_j^{\mathrm{mf}}(s), \tag{29}$$

where $E_j^{\mathrm{mf}}(s)$ is a mean-field propagator at site $j$. We use the standard mean-field approach to determine these local propagators, starting with the equation for the total propagator $E^{[m]}(s)$, Eq. (21): Assuming the above product form of the propagator, one readily obtains the equation of motion for the local mean-field propagator $E_i^{\mathrm{mf}}(s)$ by tracing out all sites except $i$ in Eq. (21). This procedure gives

$$\frac{d}{ds} E_i^{\mathrm{mf}}(s) = \mathcal{L}_i^{\mathrm{mf}}(s) E_i^{\mathrm{mf}}(s), \tag{30}$$

with initial condition $E_i^{\mathrm{mf}}(0) = \mathbb{1}$. Here, $\mathcal{L}_i^{\mathrm{mf}}(s)$ is a mean-field Lindblad operator at site $i$, which is given via

$$\mathcal{L}_i^{\mathrm{mf}}(s) E_i^{\mathrm{mf}}(s) = \mathrm{tr}_{i\pm1}\left\{ (\mathcal{L}_{i-1,i}^{\mathrm{casc}} + \mathcal{L}_{i,i+1}^{\mathrm{casc}}) \bigotimes_{j=i-1}^{i+1} E_j^{\mathrm{mf}}(s) \right\}. \tag{31}$$

Here, $\mathrm{tr}_{i\pm1}$ denotes the partial trace over sites $i-1$ and $i+1$. Straightforward algebra allows one to bring the above expression into a particular transparent form:

$$\mathcal{L}_i^{\mathrm{mf}}(s) E_i^{\mathrm{mf}}(s) = \mathcal{L}_i^{\mathrm{M}} E_i^{\mathrm{mf}}(s) - \frac{\mathbb{i}}{\hbar}[h_i(s), E_i^{\mathrm{mf}}(s)]. \tag{32}$$

Here, we introduce the notation $\mathcal{L}_i^M X = -(\mathbb{i}/\hbar)[H_{\mathrm{sys},i}, X] + \mathcal{D}[L_i]X + \mathcal{D}[R_i]X$ as well as $h_i(s) = \mathbb{i}\hbar[r_{i-1}^*(s)L_i - r_{i-1}(s)L_i^\dagger]$. In the last expression, we use the shorthand notation for the maps $r_{i-1}(s)X_{i-1} = \mathrm{tr}_{i-1}\{R_{i-1}E_{i-1}^{\mathrm{mf}}(s)X_{i-1}\}$ and $r_{i-1}^*(s)X_{i-1} = \mathrm{tr}_{i-1}\{E_{i-1}^{\mathrm{mf}}(s)X_{i-1}R_{i-1}^\dagger\}$, which map operators in the Hilbert space of replica $i-1$ (specifically, density matrices) to a c-number. Note that $\mathcal{L}_i^{\mathrm{mf}}$ is manifestly of Lindblad form. The first term in Eq. (32), $\mathcal{L}_i^M$, is in fact simply the generator of a Markovian master equation describing the replica system $i$ coupled to a bath *without* time-delayed feedback, such as a waveguide that is open on both ends. The second term captures the effect of the time-delayed feedback on a mean-field level: It generates an additional coherent evolution of the replica $i$, dependent on replica $i-1$. Specifically, one can interpret this second term as an additional coherent field driving the replica system $i$. The amplitude of this driving field is simply determined by the expectation value of the output field of the neighboring replica at site $i-1$. It is this second term that renders the mean-field equations nonlinear. Note that the mean-field equations for $E_i^{\mathrm{mf}}(s)$ depend only on $E_{i-1}^{\mathrm{mf}}(s)$ but not on $E_{i+1}^{\mathrm{mf}}(s)$. This is the direct consequence of the unidirectional nature of the cascaded chain.

With the expression (32), we can solve the nonlinear, coupled mean-field equations (30) to obtain the propagator $E^{\mathrm{mf}}(s)$ in mean-field approximation and, consequently, calculate from it the mean-field approximation of all quantities of interest as discussed in the previous sections. Figures 12(a) and 12(b) show the fidelity between the steady state in mean-field approximation and the exact steady state calculated in the previous section. As expected, the fidelity improves and approaches 1 when both the delay time and the driving increase.

Remarkably, the mean-field approximation can also capture relevant two-time correlation functions successfully: Figure 13 shows the incoherent part of the output field spectrum calculated both by the exact algorithm and using the mean-field approximation for different parameters. Again, as the driving strength and the delay time increase,

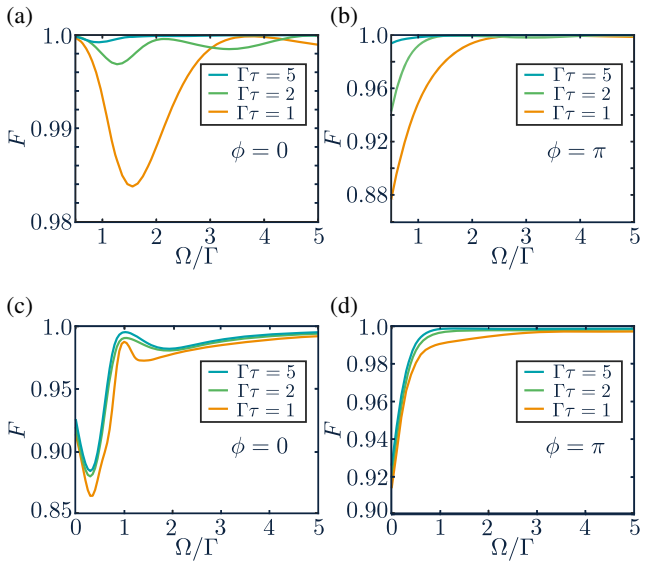


FIG. 12. Comparison of the exact steady-state solution and the mean-field approximation. (a),(b) The fidelity of the steady-state mean-field solution with the exact solution for the atom in front of the mirror [see Fig. 6(a)], $F = \left(\mathrm{tr}\sqrt{\sqrt{\rho_{\mathrm{ss}}}\rho_{\mathrm{ss}}^{\mathrm{mf}}\sqrt{\rho_{\mathrm{ss}}}}\right)^2$ [82], dependence on the driving with the delay times $\Gamma\tau = 1, 2, 5$, and (a) $\phi = 0$ and (b) $\phi = \pi$. (c),(d) The fidelity of the steady-state mean-field solution with the exact solution for two atoms interacting with a common waveguide [Fig. 6(c)]. (c) $\phi = 0$ and (d) $\phi = \pi$; $\Omega_1/\Gamma = 1$ for both plots.

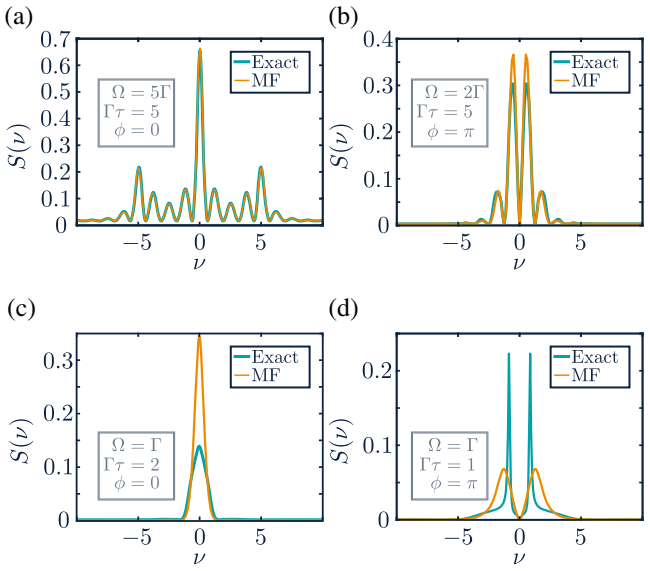


FIG. 13. Comparison of the exact steady-state solution and the mean-field approximation for the atom in front of the mirror. A comparison between the exact output field spectrum and the spectrum obtained using mean-field approximation (MF). The parameters are (a) $\Omega/\Gamma = 5$, $\Gamma\tau = 5$, and $\phi = 0$; (b) $\Omega/\Gamma = 2$, $\Gamma\tau = 5$, and $\phi = \pi$; (c) $\Omega/\Gamma = 1$, $\Gamma\tau = 2$, and $\phi = 0$; (d) $\Omega/\Gamma = 1$, $\Gamma\tau = 1$, and $\phi = \pi$. In all panels, we use $\Delta/\Gamma = 0$, $\chi = 50$, and $\Gamma\Delta t = 0.01$.

the mean-field approximation becomes more accurate. In the case of sufficiently large Rabi frequencies and delay times, the mean-field picture allows for a simple interpretation of the spectrum: It is given by the standard Mollow triplet found in the output of a strongly driven two-level system coupled to a Markovian bath [83], which is modulated with a frequency $1/\tau$ as a result of constructive (destructive) interference between the emitted photons and those returning to the atom from the delay line (previous replica).

This mean-field approach can also be applied to more complicated systems, e.g., multinode setups. In Figs. 12(c) and 12(d), we show the results of such a mean-field approximation applied to two distant, driven atoms coupled to a bidirectional waveguide [see Fig. 6(c)]. Also, in this case the mean-field ansatz reproduces the exact solution with high fidelity. This example highlights the fact that the mean-field factorization can be particularly useful in setups with multiple nodes. As mentioned above, the cost of the tensor network method developed in this work increases rapidly with the dimension of the system Hilbert space, which poses limitation for systems with multiple nodes. Whenever the mean-field approach developed in this section can be applied, this unfavorable scaling can be eliminated.

## VIII. CONCLUSION

In this work, we developed a novel approach for solving problems with continuous coherent quantum feedback involving time delays. Our method allows for numerically accurate and efficient calculations of several quantities of interest that are inaccessible with other state-of-the-art methods. Specifically, this includes parameter regimes with arbitrary time delays and direct access to steady-state properties. It is important to note that our algorithm is efficient for calculating few-body observables, such as the reduced state of the emitter(s), or few-body correlation functions of the output field (such as the spectrum or $g_2$), while the cost of accessing higher-order correlation functions grows exponentially with $n$. This is indeed consistent with the fact that it is not possible to classically simulate universal quantum computation (Ref. [16]).

In this work, we mainly focused on the minimal, nontrivial example of a system with coherent time-delayed feedback, as a way to illustrate the key concepts underlying our method and to facilitate benchmarks against other approaches. But our method could also provide a path to solve other open problems, e.g., understanding the fate of superradiance, a phenomenon in which time delays inevitably become relevant. We also envision that our methods are particularly useful to theoretically model and describe solid state quantum systems that employ inherently slow excitation carriers in on-chip quantum devices, such as surface acoustic wave phonons [28,29]. In addition, it seems plausible that the key ideas of our work can be generalized and integrated with other approaches that are used to deal with systems coupled to various forms of non-Markovian environments [53–58].

One of the most interesting challenges in going beyond the models presented in this work is to understand if it is possible to construct examples where the methods developed here fail. For instance, this could happen if one finds examples of 1D cascaded chains whose propagators are not rapidly mixing, such that the corresponding operator entanglement does not obey an area law. In this case, our method would no longer be efficient, and the computational cost would grow with the time delay. It is not clear if such dynamics exists, but recent results from the theory of isometric tensor networks (Ref. [84]) suggest that this may be possible. Identifying such setups would potentially allow one to engineer quantum optical setups that can produce qualitatively more complex output states, such as states with algebraically decaying correlation functions. This would have important implications for photonic quantum simulation approaches [22,85–87].

The datasets generated during and/or analyzed during the current study as well as the method code are available on the public repository Zenodo [88].

## ACKNOWLEDGMENTS

We thank Peter Zoller, Helmut Ritsch, and Crispin Gardiner for helpful discussions. We acknowledge financial support from the ERC Starting grant QARA (Grant No. 101041435), Horizon Europe programme HORIZON-CL4-2022-QUANTUM-02-SGA via the project

101113690 (PASQuanS2.1), and the EU-QUANTERA project TNiSQ (N-6001). This research was funded in part by the Austrian Science Fund (FWF) [grant DOI 10.55776/COE1]. The computational results presented have been achieved (in part) using the HPC infrastructure LEO of the University of Innsbruck.

## APPENDIX A: MAPPING TO 1D CASCADED CHAIN

We now prove the direct correspondence between the equation for the reduced density matrix of the atom in front of the mirror and the 1D cascaded chain. This proof can be naturally generalized to the case of multinode networks; however, for illustrational purposes, we consider here the simplest example. We start out with Eq. (14) and proceed by decomposing the superoperator $T_i$ in two superoperators $T_i^R$ and $T_i^L$, with the first one acting on both the system and the time bin $i+k$ and the second one on the system and the time bin $i$ as in Fig. 4(b): $T_i X = T_i^R T_i^L X$, where we define $T_i^R X = V_i^R X V_i^{R\dagger}$ and $T_i^L X = \mathrm{tr}_{\mathcal{H}_i}\{V_i^L X V_i^{L\dagger}\}$ with the unitary $V_i^L = \exp[-(\mathbb{i}/\hbar)H_{\mathrm{sys}}(\Delta t/2) + \Upsilon_i^L]$ and the isometry $V_i^R = \exp[-(\mathbb{i}/\hbar)H_{\mathrm{sys}}(\Delta t/2) + \Upsilon_i^R]|0\rangle_{i+k}$ correspondingly. This decomposition is correct up to Trotter errors that vanish in the $\Delta t \to 0$ limit. Note that (up to higher-order Trotter terms) this decomposition is symmetric: $T_i X = T_i^R T_i^L X = T_i^L T_i^R X$.

We rewrite Eq. (14) using the unitaries and the isometries introduced above as

$$\rho_{\mathrm{sys}}(t_n) = \mathrm{tr}_{\mathcal{H}_B}\{V_{n-1}^R V_{n-1}^L \ldots V_i^R V_i^L \ldots V_0^R V_0^L \rho_{\mathrm{sys}}(t_0) \bigotimes_{i=0}^{k-1} |0_i\rangle\langle 0_i| V_0^{L\dagger} V_0^{R\dagger} \ldots V_i^{L\dagger} V_i^{R\dagger} \ldots V_{n-1}^{L\dagger} V_{n-1}^{R\dagger}\}. \tag{A1}$$

We now carefully work out the whole expression by taking the partial trace over the bath degrees of freedom of each time bin. To do so, we introduce matrix elements of the operators $V_i^L$ and $V_i^R$ as $V_{i,b,a}^L = \langle b|V_i^L|a\rangle$ and $V_{i,a,b}^R = \langle a|V_i^R|b\rangle$, respectively, where $|a\rangle$ and $|b\rangle$ are the basis states of the $d$-dimensional system Hilbert space. Note that these matrix elements act on the photonic time bins. Specifically, $V_{i,b,a}^L$ is an operator that acts on time bin $i$, and $V_{i,a,b}^R$ is a state of the time bin $i+k$. We now can write the matrix elements of the system density matrix at time $t_n$:

$$\begin{aligned}\rho_{a_n,a_n'}^{\mathrm{sys}}(t_n) = \sum_{\mathbf{a},\mathbf{b},\mathbf{a}',\mathbf{b}'} \mathrm{tr}_{\mathcal{H}_B}\Big\{ & V_{n-1,a_n,b_{n-1}}^R V_{n-1,b_{n-1},a_{n-1}}^L \ldots V_{i,a_{i+1},b_i}^R V_{i,b_i,a_i}^L \\ & \ldots V_{0,a_1,b_0}^R V_{0,b_0,a_0}^L \rho_{a_0,a_0'}(t_0) \bigotimes_{i=0}^{k-1} |0_i\rangle\langle 0_i| V_{0,a_0',b_0'}^{L\dagger} V_{0,b_0',a_1'}^{R\dagger} \ldots V_{i,a_i',b_i'}^{L\dagger} V_{i,b_i',a_{i+1}'}^{R\dagger} \ldots V_{n-1,a_{n-1}',b_{n-1}'}^{L\dagger} V_{n-1,b_{n-1}',a_n'}^{R\dagger} \Big\},\end{aligned} \tag{A2}$$

where the sum goes over the indexes $\mathbf{a} = a_0, \ldots, a_{n-1}$, $\mathbf{b} = b_0, \ldots, b_{n-1}$, $\mathbf{a}' = a_0', \ldots, a_{n-1}'$, and $\mathbf{b}' = b_0', \ldots, b_{n-1}'$ and where we use $\rho_{a_0,a_0'}(t_0) = \langle a_0|\rho(t_0)|a_0'\rangle$. To perform the partial trace over the time bins, we rearrange the terms in the above expression, grouping together all the terms that involve the same time bin. Therefore, we group pairs $V_{i-k,a_{i-k+1},b_{i-k}}^R$ and $V_{i,b_i,a_i}^L$ (and analogously $V_{i-k,b_{i-k}',a_{i-k+1}'}^{R\dagger}$ with $V_{i,a_i',b_i'}^{L\dagger}$), since these are the only terms involving the time bin $i$. This allows us to trace out all time bins $i$ that appear in the state (i.e., the time bins from $i=0$ to $i=n+k-1$), sequentially, which gives rise to three different types of terms. The first type of terms arises from the trace over the time bins $i=0,\ldots,k-1$, which gives terms of the form

$$W_{b_i,b_i',a_i,a_i'}^{(L)} = \mathrm{tr}_{\mathcal{H}_i}\{V_{i,b_i,a_i}^L |0_i\rangle\langle 0_i| V_{i,a_i',b_i'}^{L\dagger}\}. \tag{A3}$$

The second type of terms arise from the trace over the time bins $i=k,\ldots,n-1$, which gives terms of the form

$$W_{b_i,b_i',a_{i-k+1},a_{i-k+1}',a_i,a_i',b_{i-k},b_{i-k}'}^{(LR)} = \mathrm{tr}_{\mathcal{H}_i}\{V_{i,b_i,a_i}^L V_{i-k,a_{i-k+1},b_{i-k}}^R V_{i-k,b_{i-k}',a_{i-k+1}'}^{R\dagger} V_{i,a_i',b_i'}^{L\dagger}\}. \tag{A4}$$

The third type of terms are obtained from the trace over the time bins $i=n,\ldots,n-1+k$, which gives terms of the form

$$W_{a_{i-k+1},a_{i-k+1}',b_{i-k},b_{i-k}'}^{(R)} = \mathrm{tr}_{\mathcal{H}_i}\{V_{i-k,a_{i-k+1},b_{i-k}}^R V_{i-k,b_{i-k}',a_{i-k+1}'}^{R\dagger}\}. \tag{A5}$$

To proceed, we evaluate now all three of these terms. To do so, we use the definition of $V^L$ and $V^R$ and expand to the first order in $\Delta t$ (recalling that the Ito increment $\Delta B_i$ gives contributions in the order of $\sqrt{\Delta t}$):

$$\begin{aligned}V_{i,b,a}^L = \delta_{b,a} - \frac{\mathbb{i}}{2\hbar} H_{b,a}^{\mathrm{sys}} \Delta t + (L_{b,a}\Delta B_i^\dagger - \mathrm{H.c.}) + \frac{1}{2}\Big( & (L^2)_{b,a}\Delta B_i^{\dagger 2} - (LL^\dagger)_{b,a}\Delta B_i^\dagger \Delta B_i - (L^\dagger L)_{b,a}\Delta B_i \Delta B_i^\dagger + (L^{\dagger 2})_{b,a}\Delta B_i^2\Big) \\ & + \cdots,\end{aligned} \tag{A6}$$

$$V^R_{i,a,b} = \left(\delta_{a,b} - \frac{\mathbb{i}}{2\hbar} H^{\rm sys}_{a,b}\Delta t + R_{a,b}\Delta B^\dagger_{i+k} - (R^\dagger R)_{a,b}\Delta t\right)|0_{i+k}\rangle + \frac{1}{2}(R^2)_{a,b}\Delta B^{\dagger 2}_{i+k}|0_{i+k}\rangle + \cdots. \tag{A7}$$

With this, one can evaluate the above expressions [Eqs. (A3)–(A5)] using the commutation relation of the Ito increment operator, $[\Delta B^\dagger_i, \Delta B_j] = \Delta t \delta_{ij}$. For the term (A3), we obtain to the first order in $\Delta t$

$$W^{(L)}_{b,b',a,a'} = \delta_{b,a}\delta_{b',a'} - \frac{\mathbb{i}}{2\hbar}(H_{\rm sys})_{b,a}\delta_{a',b'}\Delta t + \frac{\mathbb{i}}{2\hbar}\delta_{b,a}(H_{\rm sys})_{a',b'}\Delta t + \frac{1}{2}[2L_{b,a}L^\dagger_{a',b'} - (L^\dagger L)_{b,a}\delta_{a',b'} - \delta_{b,a}(L^\dagger L)_{a',b'}]\Delta t. \tag{A8}$$

The right-hand side can be identified with the propagator generated by a Lindblad operator $\mathcal{L}^{{\rm bd}L}$ given in Eq. (18) of the main text and written here explicitly in the basis of the system Hilbert space. To leading order in $\Delta t$, this can be rewritten as

$$W^{(L)}_{b,b',a,a'} = (e^{\Delta t \mathcal{L}^{{\rm bd}L}})_{b,b',a,a'}, \tag{A9}$$

where we define the matrix element of a superoperator as $(e^{\Delta t \mathcal{L}^{{\rm bd}L}})_{b,b',a,a'} = {\rm tr}_{\rm sys}\{|b\rangle\langle b'|(e^{\Delta t \mathcal{L}^{{\rm bd}L}})|a\rangle\langle a'|\}$. Analogously, we find for the third term (A5)

$$W^{(R)}_{a,a',b,b'} = (e^{\Delta t \mathcal{L}^{{\rm bd}R}})_{a,a',b,b'}, \tag{A10}$$

where $\mathcal{L}^{{\rm bd}R}$ is the term given in Eq. (18) in the main text. Finally, the term in Eq. (A4) can be evaluated in a similar way:

$$W^{(LR)}_{l,r,r',l'} = \delta_{l,l'}\delta_{r,r'} + \delta_{l,l'}O^{\rm sys}_{r,r'} + O^{\rm sys}_{l,l'}\delta_{r,r'} + \delta_{l,l'}O^R_{r,r'} + O^L_{l,l'}\delta_{r,r'} + O^{LR}_{l,r,r',l'}, \tag{A11}$$

where we introduce superindexes $r = \{a_{i-k+1}, b_{i-k}\}$, $l = \{b_i, a_i\}$ and $r' = \{b'_{i-k}, a'_{i-k+1}\}$, $l' = \{a'_i, b'_i\}$ (see Fig. 14). The total map is a result of different physical processes: The contributions due to the system Hamiltonian evolution are

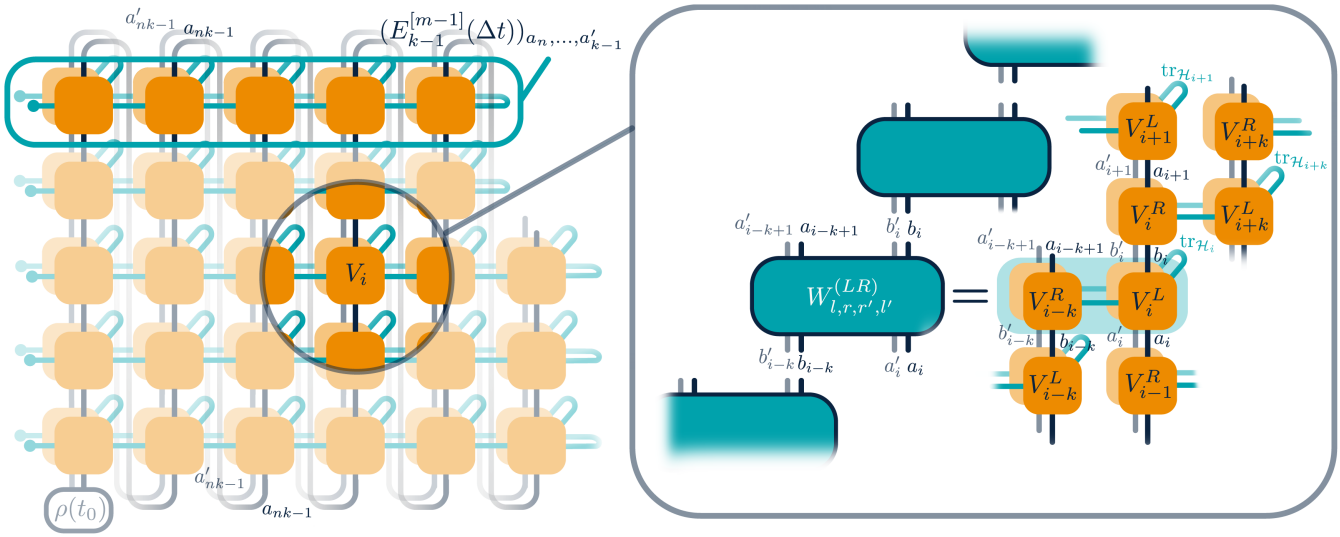


FIG. 14. Mapping to 1D cascaded chain. Reduced density matrix of the system $\rho_{\rm sys}(t_n)$ as a tensor network, the connection of the isometry $V_i$ to its neighbors is encircled and shown in detail to the right, where we separate $V^R_i$ and $V^L_i$ and explicitly write the indexes associated with each leg. Traces over the bath degrees of freedom are indicated as the contracted blue legs. Contraction of $V^R_{i-k}$ and $V^L_i$ creates local propagator $W^{(LR)}$, leading to a ladderlike structure made of these propagators for each horizontal layer in the original tensor network. Note that in the main text we use the fact that Trotter decomposition is symmetric $T_i X = T^R_i T^L_i X = T^L_i T^R_i X$ and the resulting chain of propagators has a different (zigzag) structure. In a light blue rectangle, we enclose the transfer operator $E^{[m-1]}_{k-1}(\Delta t)$ and denote the indexes through which it connects to the lowest transfer operator $E^{[m]}_0(\Delta t)$.

$$O^{\mathrm{sys}}_{r,r'} = -\frac{\mathbb{i}}{2\hbar}[(H_{\mathrm{sys}})_r\delta_{r'} - \delta_r(H_{\mathrm{sys}})_{r'}]\Delta t,$$
$$O^{\mathrm{sys}}_{l,l'} = -\frac{\mathbb{i}}{2\hbar}[(H_{\mathrm{sys}})_l\delta_{l'} - \delta_l(H_{\mathrm{sys}})_{l'}]\Delta t,$$

the dissipation through the action of the jump operator $R$,

$$O^{R}_{r,r'} = \frac{1}{2}[2R_rR^\dagger_{r'} - (R^\dagger R)_r\delta_{r'} - \delta_r(R^\dagger R)_{r'}]\Delta t,$$

and the dissipation through the action of the jump operator $L$,

$$O^{L}_{l,l'} = \frac{1}{2}[2L_lL^\dagger_{l'} - (L^\dagger L)_l\delta_{l'} - \delta_l(L^\dagger L)_{l'}]\Delta t.$$

The last contribution is a cascaded interaction between two system states:

$$O^{LR}_{l,r,r',l'} = [L_l\delta_rR^\dagger_{r'}\delta_{l'} + \delta_lR_r\delta_{r'}L^\dagger_{l'} - L^\dagger_lR_r\delta_{r'}\delta_{l'} - \delta_l\delta_rR^\dagger_{r'}L_{l'}]\Delta t.$$

We note that the total map is then a propagator generated by the cascaded Lindblad operator defined in Eq. (17) on twofold-replicated system Hilbert space:

$$W^{(LR)}_{r,l,r',l'} = W^{\mathrm{casc}}_{r,l,r',l'} = [\exp(\Delta t\mathcal{L}^{\mathrm{casc}})]_{r,l,r',l'}. \tag{A12}$$

Using the above derivations, one can trace out all the time bins in the expression (A2) and rewrite it using the three types of propagators we identified earlier:

$$\begin{aligned}\rho^{\mathrm{sys}}_{a_n,a'_n}(t_n) = \sum_{\mathbf{a},\mathbf{b},\mathbf{a}',\mathbf{b}'} & W^{(R)}_{a_n,a'_n,b_{n-1},b'_{n-1}}W^{\mathrm{casc}}_{b_{n-1},b'_{n-1},a_{n-k},a'_{n-k},a_{n-1},a'_{n-1},b_{n-1-k},b'_{n-1-k}}W^{(R)}_{a_{n-1},a'_{n-1},b_{n-2},b'_{n-2}}\\ & \ldots W^{\mathrm{casc}}_{b_{i+1},b'_{i+1},a_{i-k+2},a'_{i-k+2},a_{i+1},a'_{i+1},b_{i+1-k},b'_{i+1-k}}W^{\mathrm{casc}}_{b_i,b'_i,a_{i-k+1},a'_{i-k+1},a_i,a'_i,b_{i-k},b'_{i-k}}\\ & \ldots W^{(L)}_{b_1,b'_1,a_1,a'_1}W^{\mathrm{casc}}_{b_k,b'_k,a_1,a'_1,a_k,a'_k,b_0,b'_0}W^{(L)}_{b_0,b'_0,a_0,a'_0}\rho_{a_0,a'_0}(t_0).\end{aligned} \tag{A13}$$

This equation describes the tensor network in Fig. 14(a). This network consists of two types of transfer operators, $E^{[m]}(\Delta t)$ and $E^{[m-1]}(\Delta t)$, which we now explicitly define in terms of local propagators $W$ as

$$\begin{aligned}[E^{[p]}_i(\Delta t)]_{a_{pk+i},\ldots,a'_i} = & W^{(R)}_{a_{pk+i},a'_{pk+i},b_{pk+i-1},b'_{pk+i-1}}W^{\mathrm{casc}}_{b_{pk+i-1},b'_{pk+i-1},a_{pk+i-k},a'_{(p-1)k+i},a_{pk+i-1},a'_{pk+i-1},b_{(p-1)k+i-1},b'_{(p-1)k+i-1}}\\ & \ldots W^{\mathrm{casc}}_{b_{i+k},b'_{i+k},a_{i+1},a'_{i+1},a_{i+k},a'_{i+k},b_i,b'_i}W^{(L)}_{b_i,b'_i,a_i,a'_i},\end{aligned} \tag{A14}$$

where $p = \{m, m-1\}$. Using this, we can write the expression in Eq. (A13) using tensor network transfer operators:

$$\begin{aligned}\rho^{\mathrm{sys}}_{a_n,a'_n}(t_n) = \sum_{\mathbf{a},\mathbf{b},\mathbf{a}',\mathbf{b}'} & [E^{[m-1]}_{k-1}(\Delta t)]_{a_n,\ldots,a'_{k-1}}\ldots[E^{[m-1]}_{i_r+1}(\Delta t)]_{a_{mk+i_r+1},\ldots,a'_{i_r+1}}[E^{[m]}_{i_r}(\Delta t)]_{a_{mk+i_r},\ldots,a'_{i_r}}\\ & \ldots[E^{[m]}_1(\Delta t)]_{a_{mk+1},\ldots,a'_1}[E^{[m]}_0(\Delta t)]_{a_{mk},\ldots,a'_0}\rho_{a_0,a'_0}(t_0),\end{aligned} \tag{A15}$$

where $i_r = r/\Delta t$. Thus, a calculation of the density matrix of the atom in front of the mirror results in performing the evolution of 1D cascaded chain.

The presence of the shifted periodic boundary conditions can be shown by considering the first and the last infinitesimal propagators $E^{[m-1]}_{k-1}(\Delta t)$ and $E^{[m]}_0(\Delta t)$ in the above expression. These propagators enter the sum with the number of coinciding indexes. To see this, we can compare the indexes of two arbitrary $W^{\mathrm{casc}}$ found at the same position in the definition (A14) of both propagators: $\{b_{(n+1)k-2}, b'_{(n+1)k-2}, a_{nk-1}, a'_{nk-1}, a_{(n+1)k-2}, a'_{(n+1)k-2}, b_{nk-2}, b'_{nk-2}\}$ and $\{b_{nk-1}, b'_{nk-1}, a_{(n-1)k}, a'_{(n-1)k}, a_{nk-1}, a'_{nk-1}, b_{(n-1)k-1}, b'_{(n-1)k-1}\}$ with $n \in \mathbb{N}$. Indexes $a_{nk-1}$ and $a'_{nk-1}$ coincide, and performing summation over these indexes

leads to the contraction of the propagators $E_{k-1}^{[m-1]}(\Delta t)$ and $E_0^{[m]}(\Delta t)$, resulting in the shifted periodic boundary conditions (see also Fig. 14).

## APPENDIX B: NONVACUUM INITIAL STATE GENERALIZATION

In the main text, the method is illustrated for the vacuum initial state of the waveguide. However, it is feasible to incorporate any initial state provided it can be expressed as a product state of the local time bin states. This representation is possible, for example, for thermal, coherent, and squeezed states, among others, even if their corresponding parameters (temperature, coherent amplitude, and squeezing) depend on time. We now illustrate this generalization for the time-dependent squeezed coherent state as an example and derive the connection between the 1D cascaded chain and the atom in front of the mirror. As for the vacuum initial state, the derivations can be generalized to the case of multinode networks. We define the squeezed coherent state of the time bin $i$ as

$$|\varpi_i\rangle = |\alpha(t_i), \xi(t_i)\rangle = D[\alpha(t_i)]S[\xi(t_i)]|0_i\rangle, \quad \text{(B1)}$$

where we use displacement operator $D[\alpha(t_i)] = \exp[\alpha(t_i) \times \Delta B_i^\dagger - \alpha^*(t_i)\Delta B_i]$ and squeezing operator $S[\xi(t_i)] = \exp[\frac{1}{2}\xi^*(t_i)\Delta B_i^2 - \xi(t_i)(\Delta B_i^\dagger)^2]$ with time-dependent complex parameters $\alpha(t_i)$ and $\xi(t_i) = r(t_i)e^{\mathbb{i}\theta(t_i)}$. We now proceed by deriving an equation for the total wave function of the atom and the waveguide as in the main text [see Eq. (13)]. We form the isometry $V_i$: $\mathcal{H}_{\text{sys}} \otimes \mathcal{H}_i \to \mathcal{H}_{\text{sys}} \otimes \mathcal{H}_i \otimes \mathcal{H}_{i+k}$, which is induced by an application of the unitary map to the initial state of time bin $i+k$, $V_i = U_i|\varpi_{i+k}\rangle$.

We write the total state of the atom and the waveguide at time $t_n$ as

$$|\Psi(t_n)\rangle = V_{n-1}\ldots V_1 V_0|\phi\rangle|v\rangle, \quad \text{(B2)}$$

where $|\phi\rangle$ is the state of the system at time $t_0$, $|v\rangle = \otimes_{i=0}^{k-1}|\varpi_i\rangle$ is the initial state of the first $k$ time bins and $V_i = V_i^R V_i^L$ with $V_i^L = \exp[-(\mathbb{i}/\hbar)H_{\text{sys}}\frac{\Delta t}{2} + \Upsilon_i^L]$, and the isometry $V_i^R = \exp[-(\mathbb{i}/\hbar)H_{\text{sys}}(\Delta t/2) + \Upsilon_i^R]|0\rangle_{i+k}$.

The reduced density operator at time $t_n$ is given by $\rho_{\text{sys}}(t_n) = \text{tr}_{\mathcal{H}_B}\{|\Psi(t_n)\rangle\langle\Psi(t_n)|\}$.

As in Appendix A, we can write the matrix elements of the system density matrix at time $t_n$ based on Eq. (B2):

$$\rho^{\text{sys}}_{a_n,a_n'}(t_n) = \sum_{\mathbf{a},\mathbf{b},\mathbf{a}',\mathbf{b}'} \text{tr}_{\mathcal{H}_B}\Big\{V^R_{n-1,a_n,b_{n-1}} V^L_{n-1,b_{n-1},a_{n-1}} \ldots V^R_{i,a_{i+1},b_i} V^L_{i,b_i,a_i} \ldots V^R_{0,a_1,b_0} V^L_{0,b_0,a_0} \rho_{a_0,a_0'}(t_0) \bigotimes_{i=0}^{k-1} |\varpi_i\rangle\langle\varpi_i| V^{L\dagger}_{0,a_0',b_0'} V^{R\dagger}_{0,b_0',a_1'} \ldots V^{L\dagger}_{i,a_i',b_i'} V^{R\dagger}_{i,b_i',a_{i+1}'} \ldots V^{L\dagger}_{n-1,a_{n-1}',b_{n-1}'} V^{R\dagger}_{n-1,b_{n-1}',a_n'}\Big\}, \quad \text{(B3)}$$

where the sum goes over the indexes $\mathbf{a} = a_0, \ldots, a_{n-1}$, $\mathbf{b} = b_0, \ldots, b_{n-1}$, $\mathbf{a}' = a_0', \ldots, a_{n-1}'$, and $\mathbf{b}' = b_0', \ldots, b_{n-1}'$ and where we use $\rho_{a_0,a_0'}(t_0) = \langle a_0|\rho(t_0)|a_0'\rangle$. Again, we rearrange the terms in the above expression, grouping together all the terms that involve the same time bin, which gives rise to three different types of terms. The first type of terms arises from the trace over the time bins $i = 0, \ldots, k-1$, which gives terms of the form

$$W^{(L)}_{b_i,b_i',a_i,a_i'} = \text{tr}_{\mathcal{H}_i}\{V^L_{i,b_i,a_i}|\varpi_i\rangle\langle\varpi_i|V^{L\dagger}_{i,a_i',b_i'}\}. \quad \text{(B4)}$$

The second type of terms arise from the trace over the time bins $i = k, \ldots, n-1$, which gives terms of the form

$$W^{(LR)}_{b_i,b_i',a_{i-k+1},a_{i-k+1}',a_i,a_i',b_{i-k},b_{i-k}'} = \text{tr}_{\mathcal{H}_i}\Big\{V^L_{i,b_i,a_i} V^R_{i-k,a_{i-k+1},b_{i-k}} V^{R\dagger}_{i-k,b_{i-k}',a_{i-k+1}'} V^{L\dagger}_{i,a_i',b_i'}\Big\}. \quad \text{(B5)}$$

The third type of terms are obtained from the trace over the time bins $i = n, \ldots, n-1+k$, which gives terms of the form

$$W^{(R)}_{a_{i-k+1},a_{i-k+1}',b_{i-k},b_{i-k}'} = \text{tr}_{\mathcal{H}_i}\Big\{V^R_{i-k,a_{i-k+1},b_{i-k}} V^{R\dagger}_{i-k,b_{i-k}',a_{i-k+1}'}\Big\}. \quad \text{(B6)}$$

We first consider Eq. (B4) and insert the identity $\mathbb{1} = D[\alpha(t_i)]S[\xi(t_i)]S^\dagger[\xi(t_i)]D^\dagger[\alpha(t_i)]$:

$$W^{(L)}_{b_i,b_i',a_i,a_i'} = \text{tr}_{\mathcal{H}_i}\{D[\alpha(t_i)]S[\xi(t_i)]\tilde{V}^L_{i,b_i,a_i}|0_i\rangle\langle 0_i|\tilde{V}^{L\dagger}_{i,b_i,a_i} S^\dagger[\xi(t_i)]D^\dagger[\alpha(t_i)]\}, \quad \text{(B7)}$$

where we define $\tilde{V}_i^L = S^\dagger[\xi(t_i)]D^\dagger[\alpha(t_i)]V_i^L D[\alpha(t_i)]S[\xi(t_i)]$. After using the permutation property of the trace, we arrive at the expression analogous to Eq. (A3):

$$W^{(L)}_{b_i,b_i',a_i,a_i'} = \text{tr}_{\mathcal{H}_i}\{\tilde{V}^L_{i,b_i,a_i}|0_i\rangle\langle 0_i|\tilde{V}^{L\dagger}_{i,b_i,a_i}\}. \quad \text{(B8)}$$

We now use the fact that $S^\dagger[\xi(t_i)]D^\dagger[\alpha(t_i)]\Delta B_i D[\alpha(t_i)]S[\xi(t_i)] = \Delta B_i \cosh r(t_i) - e^{\mathbb{i}\theta(t_i)}\Delta B_i^\dagger \sinh r(t_i) + \alpha(t_i)\Delta t$ to expand $\tilde{V}_i^L$:

$$\begin{aligned}
\tilde{V}_i^L &= S^\dagger[\xi(t_i)]D^\dagger[\alpha(t_i)]\exp\left(-\frac{\mathbb{i}}{\hbar}H_{\mathrm{sys}}\frac{\Delta t}{2} + \Upsilon_i^L\right)D[\alpha(t_i)]S[\xi(t_i)] \\
&= \exp\left(-\frac{\mathbb{i}}{\hbar}H_{\mathrm{sys}}\frac{\Delta t}{2} + \left[LS^\dagger[\xi(t_i)]D^\dagger[\alpha(t_i)]\Delta B_i^\dagger D[\alpha(t_i)]S[\xi(t_i)] - \mathrm{H.c.}\right]\right) \\
&= \exp\left(-\frac{\mathbb{i}}{\hbar}H_{\mathrm{sys}}\frac{\Delta t}{2} + \left[L[\Delta B_i \cosh r(t_i) - e^{\mathbb{i}\theta(t_i)}\Delta B_i^\dagger \sinh r(t_i) + \alpha(t_i)\Delta t] - \mathrm{H.c.}\right]\right) \\
&= \exp\left(-\frac{\mathbb{i}}{\hbar}H_{\mathrm{sys}}\frac{\Delta t}{2} + \left[\alpha(t_i)L\Delta t + [\cosh r(t_i)L - e^{\mathbb{i}\theta(t_i)}\sinh r(t_i)L^\dagger]\Delta B_i - \mathrm{H.c.}\right]\right) \\
&= \exp\left(-\frac{\mathbb{i}}{\hbar}\tilde{H}_{\mathrm{sys}}(t_i)\frac{\Delta t}{2} + \left[\tilde{L}(t_i)\Delta B_i - \mathrm{H.c.}\right]\right) = \mathbb{1} - \frac{\mathbb{i}}{2\hbar}\tilde{H}_{\mathrm{sys}}(t_i)\Delta t + [\tilde{L}(t_i)\Delta B_i^\dagger - \mathrm{H.c.}] \\
&\quad + \frac{1}{2}\left([\tilde{L}(t_i)^2]\Delta B_i^{\dagger 2} - [\tilde{L}(t_i)\tilde{L}^\dagger(t_i)]\Delta B_i^\dagger \Delta B_i - [\tilde{L}^\dagger(t_i)\tilde{L}(t_i)]\Delta B_i \Delta B_i^\dagger + [\tilde{L}^{\dagger 2}(t_i)]\Delta B_i^2\right) + \cdots,
\end{aligned} \tag{B9}$$

where we define $\tilde{H}_{\mathrm{sys}}(t_i) = H_{\mathrm{sys}} + 2\mathbb{i}\hbar[\alpha(t_i)L - \alpha^*(t_i)L]$ as well as $\tilde{L}(t_i) = \cosh r(t_i)L - e^{-\mathbb{i}\theta(t_i)}\sinh r(t_i)L^\dagger$ and expand the exponent to the first order in $\Delta t$. The operator $\tilde{L}$ is a redefined system operator that now depends on time. The expression in Eq. (B9) is analogous to the one in Eq. (A6), and, therefore, $W^{(L)}$ is again a propagator generated by a Lindblad operator in the form of $\mathcal{L}^{\mathrm{bd}L}$ given in Eq. (18) with a redefined expression for system Hamiltonian and system operators:

$$\begin{aligned}
W^{(L)}_{b_i,b_i',a_i,a_i'} &= \delta_{b_i,a_i}\delta_{b_i',a_i'} - \frac{\mathbb{i}}{2\hbar}[\tilde{H}_{\mathrm{sys}}(t_i)]_{b_i,a_i}\delta_{a_i',b_i'}\Delta t + \frac{\mathbb{i}}{2\hbar}\delta_{b_i,a_i}[\tilde{H}_{\mathrm{sys}}(t_i)]_{a_i',b_i'}\Delta t \\
&\quad + \frac{1}{2}\{2\tilde{L}(t_i)_{b_i,a_i}\tilde{L}(t_i)^\dagger_{a_i',b_i'} - [\tilde{L}(t_i)^\dagger\tilde{L}(t_i)]_{b_i,a_i}\delta_{a_i',b_i'} - \delta_{b_i,a_i}[\tilde{L}(t_i)^\dagger\tilde{L}(t_i)]_{a_i',b_i'}\}\Delta t \\
&= \delta_{b_i,a_i}\delta_{b_i',a_i'} - \frac{\mathbb{i}}{2\hbar}(H_{\mathrm{sys}})_{b_i,a_i}\delta_{a_i',b_i'}\Delta t + \frac{\mathbb{i}}{2\hbar}\delta_{b_i,a_i}(H_{\mathrm{sys}})_{a_i',b_i'}\Delta t + \alpha(t_i)L_{b,a}\delta_{a',b'}\Delta t - \delta_{b,a}\alpha^*(t_i)L^\dagger_{a',b'}\Delta t \\
&\quad + \frac{(1+\mathcal{N}_i)}{2}[2L_{b_i,a_i}L^\dagger_{a_i',b_i'} - (L^\dagger L)_{b_i,a_i}\delta_{a_i',b_i'} - \delta_{b_i,a_i}(L^\dagger L)_{a_i',b_i'}]\Delta t \\
&\quad + \frac{\mathcal{N}_i}{2}[2L^\dagger_{b_i,a_i}L_{a_i',b_i'} - (LL^\dagger)_{b_i,a_i}\delta_{a_i',b_i'} - \delta_{b_i,a_i}(LL^\dagger)_{a_i',b_i'}]\Delta t \\
&\quad - \frac{\mathcal{M}_i}{2}[2L^\dagger_{b_i,a_i}L_{a_i',b_i'}L^\dagger_{a_i',b_i'} - (L^\dagger)^2_{b_i,a_i}\delta_{a_i',b_i'} - \delta_{b_i,a_i}(L^\dagger)^2_{a_i',b_i'}]\Delta t - \frac{\mathcal{M}_i^*}{2}[2L_{b_i,a_i}L_{a_i',b_i'} - L^2_{b_i,a_i}\delta_{a_i',b_i'} - \delta_{b_i,a_i}L^2_{a_i',b_i'}]\Delta t,
\end{aligned} \tag{B10}$$

where we introduce the number of quanta $\mathcal{N}_i$ in time bin $i$ and the corresponding squeezing measure $\mathcal{M}_i$ in each time bin, respectively, as

$$\begin{aligned}
\mathcal{N}_i &= \sinh^2 r(t_i), \\
\mathcal{M}_i &= -e^{\mathbb{i}\theta(t_i)}\sinh r(t_i)\cosh r(t_i).
\end{aligned} \tag{B11}$$

We proceed with the expression in Eq. (B5) and perform the steps analogous to those used in derivation of Eq. (B10). After inserting identities $\mathbb{1} = D[\alpha(t_i)]S[\xi(t_i)]S^\dagger[\xi(t_i)]D^\dagger[\alpha(t_i)]$ and using the permutation property of the trace, we obtain

$$W^{(LR)}_{b_i,b_i',a_{i-k+1},a_{i-k+1}',a_i,a_i',b_{i-k},b_{i-k}'} = \mathrm{tr}_{\mathcal{H}_i}\{\tilde{V}^L_{i,b_i,a_i}\tilde{V}^R_{i-k,a_{i-k+1},b_{i-k}}\tilde{V}^{R\dagger}_{i-k,b_{i-k}',a_{i-k+1}'}\tilde{V}^{L\dagger}_{i,a_i',b_i'}\}. \tag{B12}$$

The operator $\tilde{V}^L$ is given in Eq. (B9), and analogously we define $\tilde{V}^R_{i-k} = S^\dagger[\xi(t_i)]D^\dagger[\alpha(t_i)]V^R_{i-k}$. The latter can be expanded as

$$\tilde{V}^R_{i-k} = S^\dagger[\xi(t_i)]D^\dagger[\alpha(t_i)]\exp\left(-\frac{\mathbb{i}}{\hbar}H_{\rm sys}\frac{\Delta t}{2}+\Upsilon^R_{i-k}\right)D[\alpha(t_i)]S[\xi(t_i)]|0\rangle_i$$
$$= \left(\mathbb{1}-\frac{\mathbb{i}}{2\hbar}\tilde{H}_{\rm sys}(t_i)\Delta t+\tilde{R}(t_i)\Delta B_i^\dagger-[\tilde{R}(t_i)^\dagger\tilde{R}(t_i)]\Delta t\right)|0_i\rangle+\frac{1}{2}[\tilde{R}(t_i)^2]\Delta B_i^{\dagger 2}|0_i\rangle+\cdots \tag{B13}$$

with the redefined system operator $\tilde{R}(t_i)=\cosh r(t_i)R-e^{-\mathbb{i}\theta(t_i)}\sinh r(t_i)R^\dagger$. Thus, the expression in Eq. (B12) is a propagator generated by the cascaded Lindblad operator in the form defined in Eq. (17) on twofold-replicated system Hilbert space with the redefined system Hamiltonian and system operators:

$$W^{(LR)}_{l,r,r',l'}=\delta_{l,l'}\delta_{r,r'}+\delta_{l,l'}\tilde{O}^{\rm sys}_{r,r'}+\tilde{O}^{\rm sys}_{l,l'}\delta_{r,r'}+\delta_{l,l'}\tilde{O}^R_{r,r'}+\tilde{O}^L_{l,l'}\delta_{r,r'}+\tilde{O}^{LR}_{l,r,r',l'}, \tag{B14}$$

where we introduce superindexes $r=\{a_{i-k+1},b_{i-k}\}$, $l=\{b_i,a_i\}$ and $r'=\{b'_{i-k},a'_{i-k+1}\}$, $l'=\{a'_i,b'_i\}$. The above expression is a sum of different operators. The contributions due to the system Hamiltonian evolution for both replicas are

$$\tilde{O}^{\rm sys}_{r,r'}=-\frac{\mathbb{i}}{2\hbar}[(H_{\rm sys})_r\delta_{r'}-\delta_r(H_{\rm sys})_{r'}]\Delta t+\alpha(t_i)R_{b,a}\delta_{a',b'}\Delta t-\delta_{b,a}\alpha^*(t_i)R^\dagger_{a',b'}\Delta t,$$
$$\tilde{O}^{\rm sys}_{l,l'}=-\frac{\mathbb{i}}{2\hbar}[(H_{\rm sys})_l\delta_{l'}-\delta_l(H_{\rm sys})_{l'}]\Delta t+\alpha(t_i)L_{b,a}\delta_{a',b'}\Delta t-\delta_{b,a}\alpha^*(t_i)L^\dagger_{a',b'}\Delta t.$$

The interaction of the first replica with the right-moving modes is given by

$$\tilde{O}^R_{r,r'}=\frac{(1+\mathcal{N}_i)}{2}[2R_rR^\dagger_{r'}-(R^\dagger R)_r\delta_{r'}-\delta_r(R^\dagger R)_{r'}]\Delta t+\frac{\mathcal{N}_i}{2}[2R^\dagger_rR_{r'}-(RR^\dagger)_r\delta_{r'}-\delta_r(RR^\dagger)_{r'}]\Delta t$$
$$-\frac{\mathcal{M}_i}{2}[2R^\dagger_rR^\dagger_{r'}-(R^\dagger)^2_r\delta_{r'}-\delta_r(R^\dagger)^2_{r'}]\Delta t-\frac{\mathcal{M}^*_i}{2}[2R_rR_{r'}-R^2_r\delta_{r'}-\delta_rR^2_{r'}]\Delta t.$$

The interaction of the second replica with the left-moving modes is given by

$$\tilde{O}^{\rm L}_{l,l'}=\frac{(1+\mathcal{N}_i)}{2}[2L_lL^\dagger_{l'}-(L^\dagger L)_l\delta_{l'}-\delta_l(L^\dagger L)_{l'}]\Delta t+\frac{\mathcal{N}_i}{2}[2L^\dagger_lL_{l'}-(LL^\dagger)_l\delta_{l'}-\delta_l(LL^\dagger)_{l'}]\Delta t$$
$$-\frac{\mathcal{M}_i}{2}[2L^\dagger_lL^\dagger_{l'}-(L^\dagger)^2_l\delta_{l'}-\delta_l(L^\dagger)^2_{l'}]\Delta t-\frac{\mathcal{M}^*_i}{2}[2L_lL_{l'}-L^2_l\delta_{l'}-\delta_lL^2_{l'}]\Delta t.$$

The cascaded interaction between the two replicas is

$$\tilde{O}^{LR}_{l,r,r',l'}=(1+\mathcal{N}_i)[L_l\delta_rR^\dagger_{r'}\delta_{l'}+\delta_lR_r\delta_{r'}L^\dagger_{l'}-L^\dagger_lR_r\delta_{r'}\delta_{l'}-\delta_l\delta_rR^\dagger_{r'}L_{l'}]\Delta t+\mathcal{N}_i[L^\dagger_l\delta_rR_{r'}\delta_{l'}+\delta_lR^\dagger_r\delta_{r'}L_{l'}-L_lR^\dagger_r\delta_{r'}\delta_{l'}$$
$$-\delta_l\delta_rR_{r'}L^\dagger_{l'}]\Delta t-\mathcal{M}_i[L^\dagger_l\delta_rR^\dagger_{r'}\delta_{l'}+\delta_lR^\dagger_r\delta_{r'}L^\dagger_{l'}-L^\dagger_lR^\dagger_r\delta_{r'}\delta_{l'}-\delta_l\delta_rR^\dagger_{r'}L^\dagger_{l'}]\Delta t-\mathcal{M}^*_i[L_l\delta_rR_{r'}\delta_{l'}+\delta_lR_r\delta_{r'}L_{l'}$$
$$-L_lR_r\delta_{r'}\delta_{l'}-\delta_l\delta_rR_{r'}L_{l'}]\Delta t.$$

It is easy to show that the term $W^{(R)}$ given in Eq. (B6) is also a propagator generated by a Lindblad operator in the form of $\mathcal{L}^{{\rm bd}R}$ given in Eq. (18) with the redefined expression for the system Hamiltonian and system operators. The three types of propagators described above combined together describe the evolution of 1D cascaded chain and the density matrix given in Eq. (B3) can be obtained using the methods described in Sec. IV.

## APPENDIX C: INFINITE CHAIN ALGORITHM

As discussed in the main text in Sec. IV B, the steady state of the atom in front of the mirror can be accessed by calculating the propagator of the infinite 1D cascaded chain. To do so, we make a translational invariant ansatz where all tensors are identical independently of the site they are associated with, $C^{[k]}(s)=C(s)$. We solve Eq. (21) for this transitionally invariant infinite system size propagator using the infinite time-evolving block decimation algorithm (iTEBD) [76]. This is done using a two-site unit cell, with tensors denoted by $A(s)$ and $B(s)$ for even and odd sites, respectively. The integration of Eq. (21) is achieved in a Trotterized fashion, where at each integration step we first apply $W_{\rm casc}$ to $A$ and $B$, then exchange the tensors, and apply $W_{\rm casc}$ to $B$ and $A$. Note that this construction leads to tensors that are identical up to the Trotter errors: $A(\tau)=B(\tau)=C(\tau)$.

Once the infinite system size propagator is obtained, the density matrix of the atom in front of the mirror in the steady state, $\rho_{\rm ss}$, is obtained by a contraction with shifted periodic boundary conditions; see Eq. (24). To perform

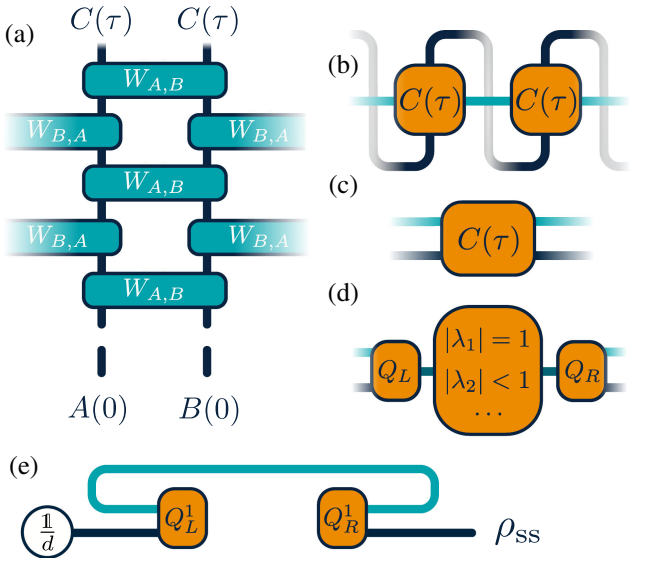


FIG. 15. The infinite 1D chain algorithm. (a) Two tensors $A(0)$ and $B(0)$ are evolved until time $\tau$ using iTEBD by applying two-site superoperators $W_{A,B}$ and $W_{B,A}$; (b) acquired after this evolution, identical tensors $C(\tau)$ are contracted together. To achieve that, we first rearrange the legs of the tensor $C(\tau)$ (c) and then apply spectral decomposition (d), where $Q_L$ and $Q_R$ are matrices consisting of the left and right eigenvectors, respectively. To calculate $\rho_{\rm ss}$, we contract an infinite number of the decomposed tensors; therefore, only vectors $Q_L^1$ and $Q_R^1$ associated with the eigenvalue $|\lambda_1| = 1$ are left to be contracted (e).

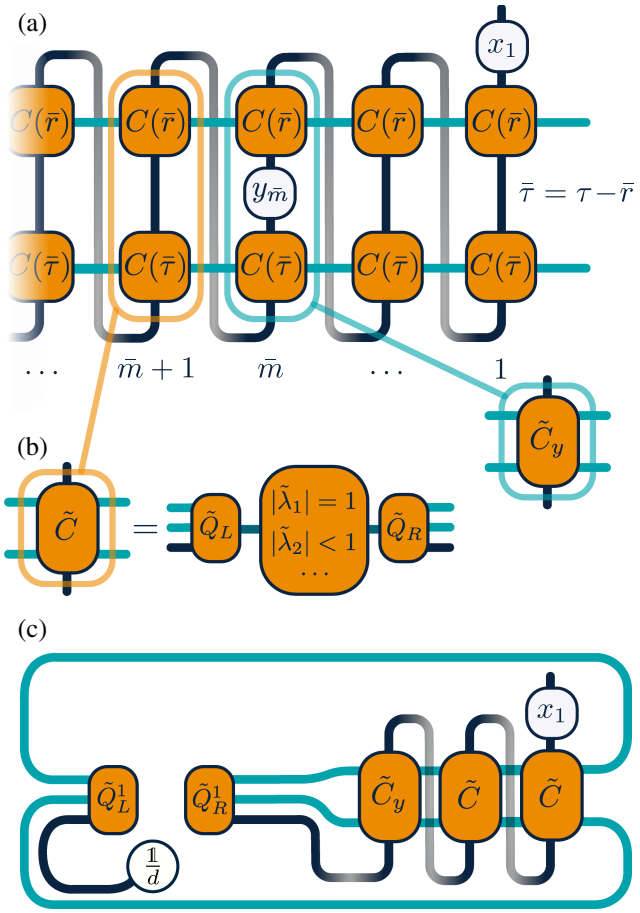


FIG. 16. Steady-state two-times correlation function algorithm. (a) To calculate the system correlation function, we first apply the system operators to two semi-infinite propagators with propagating times $\bar{\tau} = \tau - \bar{r}$ and $\bar{r}$ and then contract the whole structure with the shifted periodic boundary conditions. (b) The contraction is performed using the spectral decomposition of a combined transfer operator $\tilde{C}$ comprising $C(\bar{r})$ and $C(\bar{\tau})$ contracted over the physical leg. $\tilde{C}$ is again a completely positive trace-preserving map with $|\tilde{\lambda}_1| = 1$. (c) We then contract an infinite number of $\tilde{C}$ with $\rho = (1/d)$ and the rest tensor structure on the right and then trace over the virtual degrees of freedom. When taking the trace over the system degrees of freedom of the resulting structure, we obtain the correlation function $\lim_{t\to\infty}\langle x(t)y(t-t')\rangle$.

this contraction, we first reshape the tensor $C(\tau)$ such that it forms a square matrix of dimension $\chi d^2 \times \chi d^2$ and subsequently calculate its eigenvalues $\lambda_\alpha$ as well as the matrices containing left and right eigenvectors, $Q_L$ and $Q_R$ [cf. Figs. 15(c) and 15(d)], i.e., $C(s) = \sum_\alpha (Q_L)_\alpha \lambda_\alpha (Q_R)_\alpha$. Introducing the diagonal matrix $\Lambda_{\alpha,\beta} = \delta_{\alpha,\beta}\lambda_\alpha$, the steady state is given by $\rho_{\rm ss} = {\rm tr}_{\rm virt}\{\lim_{m\to\infty} C^m\} = {\rm tr}_{\rm virt}\{\lim_{m\to\infty} Q_L \Lambda^m Q_R\}\mathbb{1}/d$, where we introduce ${\rm tr}_{\rm virt}\{\cdots\}$ representing the trace over the virtual degrees of freedom [see Fig. 15(e)]. Since $C(\tau)$ is a completely positive trace-preserving map, its largest eigenvalue is of magnitude one, i.e., $|\lambda_1| = 1$. If the steady state is unique, all other eigenvalues are smaller, i.e., $|\lambda_k| < 1$ (for $k = 2, 3, \ldots$). Therefore, we can easily perform the total contraction in the infinite limit, obtaining $\rho_{\rm ss} = {\rm tr}_{\rm virt}\{\lim_{m\to\infty} Q_L D^m Q_R\} = Q_L^1 Q_R^1 \mathbb{1}/d$, where $Q_L^1$ and $Q_R^1$ are the left and the right eigenvector, respectively, associated with the eigenvalue $|\lambda_1| = 1$.

Another useful feature of the above procedure is that we can compute the time required to achieve the steady state $t_{\rm ss}$. Specifically, we can bound this time via the second-largest eigenvalue of the transfer tensor $C(\tau)$, $|\lambda_2|^{\lceil t_{\rm ss}/\tau \rceil} = \exp(-t/t_{\rm ss})$, which describes how fast the information about the initial state fades with time (the number of sites in the chain). Thus, we obtain the steady-state time as

$$t_{\rm ss} = -2\frac{\tau}{\log_2 |\lambda_2|}. \tag{C1}$$

Arbitrary system correlation functions as well as field correlation functions (using input-output formalism) can be calculated in the infinite limit in a similar way as in the case of the transient dynamics. Let us consider the example of two-times system correlation function $\lim_{t\to\infty}\langle x(t)y(t-t')\rangle$. This expression depends only on the time difference $t' = \bar{m}\tau + \bar{r}$. Again, we can write $\lim_{t\to\infty}\langle x(t)y(t-t')\rangle = {\rm tr}\{\mathcal{P}(M^{[\infty]})(\mathbb{1}/d)\}$ with $M^{[\infty]}$ defined as

$$M^{[\infty]} = x_1 E^{[\infty]}(\bar{r}) y_{\bar{m}} E^{[\infty]}(\tau - \bar{r}), \tag{C2}$$

where we use propagator $E^{[\infty]}(t')$ defined as a propagator of 1D semi-infinite cascaded chain with infinitely many sites on the left. In contrast to the finite chain algorithm, here we count sites from the right (finite) side of the chain; thus, $x_1$ denotes the operator $x$ acting on the rightmost replica in the chain and $y_{\bar{m}}$ acts on the replica located $\bar{m}$ sites away from the right as illustrated in Fig. 16. We perform the contraction of the infinite side of the chain again by means of the spectral decomposition. As for the transient case, the computational cost of calculating the steady-state $p$-times correlation function scales exponentially with $p$.

## APPENDIX D: MULTINODE SETUPS

### 1. Multinode setups connected unidirectionally

We now provide details on the generalization of the analysis described in the main text for the case of the multiple-node networks discussed in the main text. First, we consider the case of two nodes coupled to a bidirectional waveguide. Note that this setup can be equivalently interpreted as a network of two nodes (denoted $A$ and $B$) coupled to two unidirectional waveguides, where these waveguides represent the left- and the right-moving photons of the bidirectional waveguide, respectively. We also generalize our algorithm to the case of $n$ nodes interacting with $n$ unidirectional waveguides in setups of the form given in Fig. 6 for $n = 3$. In each of these cases, time delays lead to an essential non-Markovianity due to the possibility of information to propagating in loops with time delays. Surprisingly, any multinode problem with commensurate round-trip times between the nodes mediated by the unidirectional channel can be mapped to a set of Markovian 1D cascaded chains; e.g., the two-node problem maps to the evolution of two 1D cascaded chains, and, consequently, the three-node setup corresponds to the three 1D cascaded chains.

To start, let us consider the case of the two connected nodes shown in Fig. 2(b). For this configuration, one can again build a tensor network representing the total wave function $|\Psi(t)\rangle$ of both nodes and the state of the waveguide. Similar to the single-node case, one can obtain the tensor network for the reduced density matrix of both nodes by tracing out the bath degrees of freedom $\rho_{\mathrm{sys}}(t) = \mathrm{tr}_{\mathcal{H}_B}\{|\Psi(t)\rangle\langle\Psi(t)|\}$. The size of this network along the first dimension is set by $2k$, i.e., by the round-trip time $2\tau$ in units of $\Delta t$, while the size along the second dimension is given by $m = \lceil n/k \rceil$, i.e., total evolution time $t_n - t_0$ in units of the time $\tau$, rounded up. Again, we identify the transfer operator of the total network. For this network, we find that there are two relevant transfer operators: These operators are the propagators describing the evolution of two 1D cascaded chains. The first chain consists of replicas of node $A$ on odd sites and replicas of node $B$ on even sites ($ABABAB\ldots$), and the second chain has opposite order ($BABABA\ldots$). We therefore call the first chain $AB$ chain and the second chain $BA$ chain. Each chain has $m$ replicas, where $m$ is defined again through $t_n = m\tau + r$, with $0 \le r \le \tau$ [see Fig. 6(c)]. The corresponding propagators for these chains satisfy the following equations [analogous to Eq. (21)]:

$$\frac{d}{ds} E^{[m]}_{\{AB\}}(s) = \mathcal{L}^{[m]}_{\{AB\}} E^{[m]}_{\{AB\}}(s), \tag{D1}$$

$$\frac{d}{ds} E^{[m]}_{\{BA\}}(s) = \mathcal{L}^{[m]}_{\{BA\}} E^{[m]}_{\{BA\}}(s), \tag{D2}$$

with the Lindblad superoperators defined as

$$\mathcal{L}^{[m]}_{\{AB\}} = \sum_{j\in\mathrm{odd}} \mathcal{L}^{\mathrm{casc}}_{A,B} + \sum_{j\in\mathrm{even}} \mathcal{L}^{\mathrm{casc}}_{B,A} + \mathcal{L}^{\mathrm{boundary}}_{\{AB\}}, \tag{D3}$$

$$\mathcal{L}^{[m]}_{\{BA\}} = \sum_{j\in\mathrm{odd}} \mathcal{L}^{\mathrm{casc}}_{B,A} + \sum_{j\in\mathrm{even}} \mathcal{L}^{\mathrm{casc}}_{A,B} + \mathcal{L}^{\mathrm{boundary}}_{\{BA\}}, \tag{D4}$$

where the summation goes over odd (even) $j$ from 1 to $m-1$ and $\mathcal{L}^{\mathrm{casc}}_{A,B}$ ($\mathcal{L}^{\mathrm{casc}}_{B,A}$) describes a cascaded coupling from replica $A$ to replica $B$ (from $B$ to $A$):

$$\mathcal{L}^{\mathrm{casc}}_{A,B} X = -\frac{\mathbb{i}}{\hbar}[H^{\mathrm{casc}}_{A,B}, X] + \mathcal{D}[R_A + L_B]X, \tag{D5}$$

with the cascaded Hamiltonian

$$H^{\mathrm{casc}}_{A,B} = \frac{1}{2}(H_{\mathrm{sys},A} + H_{\mathrm{sys},B} + \mathbb{i}(R_A^\dagger L_B - L_B^\dagger R_A))$$

and analogously

$$\mathcal{L}^{\mathrm{casc}}_{B,A} X = -\frac{\mathbb{i}}{\hbar}[H^{\mathrm{casc}}_{B,A}, X] + \mathcal{D}[R_B + L_A]X, \tag{D6}$$

with the cascaded Hamiltonian

$$H^{\mathrm{casc}}_{B,A} = \frac{1}{2}\left(H_{\mathrm{sys},B} + H_{\mathrm{sys},A} + \mathbb{i}(R_B^\dagger L_A - L_A^\dagger R_B)\right).$$

The expression Eq. (D3) also contains boundary terms $\mathcal{L}^{\mathrm{boundary}}_{\{AB\}}$ and $\mathcal{L}^{\mathrm{boundary}}_{\{BA\}}$ acting on the first and the last replica of each chain, analogous to Eq. (18).

To calculate the reduced density matrix of the nodes $A$ and $B$ at time $t_n$, we calculate the total propagators for the two chains, contract them with each other and with double-shifted periodic boundary conditions, and then apply the result to the initial density matrix [see Fig. 6(d)]:

$$\rho^{AB}_{\mathrm{sys}}(t_n) = \mathcal{P}_2\left[E^{[m-1]}_{\{\mathrm{AB}\}}(\tau - r) E^{[m]}_{\{\mathrm{AB}\}}(r) E^{[m-1]}_{\{\mathrm{BA}\}}(\tau - r) E^{[m]}_{\{\mathrm{BA}\}}(r)\right] \rho^{AB}_{\mathrm{sys}}(t_0), \tag{D7}$$

where we use $\mathcal{P}_2(X)$ to denote an application of the double-shifted periodic boundary conditions to the tensor network $X$. The cost of the total contraction in Eq. (D7) is $O(m\chi^5 d^6)$.

Note that one could also calculate one total propagator of one chain of length $m+1$ ($ABABAB\ldots$) by first applying the cascaded Lindblad propagators to the sites $2,\ldots,m$ until time $r$, then propagating only sites $2,\ldots,m-1$ until time $\tau$, followed by the evolution of sites $1,\ldots,m-1$ for time $r$, and finally evolving the sites $1,\ldots,m-2$ for time $\tau-r$ [cf. Fig. 6(d)]. The resulting propagator is again contracted with the double-shifted periodic boundary conditions and the initial density matrix at a computational cost of $O(m\chi^2 d^6)$. Even though this approach is more efficient for calculating the density matrix at a fixed time $t_n$, it requires iterating the entire calculation for each different time of interest. In contrast, the method described above allows one to compute the propagators for a fixed $\tau$ in parallel and then construct tensor networks for the various times of interest, tracing out the last replicas if needed during the process. This discussion applies to the calculation of the correlation functions described in the main text: One can evolve the cascaded chain and insert operators $x$ and $y$ at the right places during the evolution. The algorithm in the end must be chosen based on the specific task.

In the case of three nodes $A$, $B$, and $C$ connected in a loop via unidirectional waveguides [see Fig. 6(e)], the total tensor network for the reduced density matrix has three types of transfer operators. These operators are propagators for three cascaded chains consisting of replicas of the nodes: ($ABCABCABC\ldots$), ($CABCABCAB\ldots$), and ($BCABCABCA\ldots$), as illustrated in Fig. 6(e). The three resulting total propagators are contracted with the triple-shifted periodic boundary conditions and applied to the initial system density matrix $\rho_{ABC}(t_0)$ as depicted in Fig. 6(f):

$$\rho_{\mathrm{sys}}^{ABC}(t_n)=\mathcal{P}_3[E^{[m-1]}_{\{\mathrm{ABC}\}}(\tau-r)E^{[m]}_{\{\mathrm{ABC}\}}(r)E^{[m-1]}_{\{\mathrm{CAB}\}}(\tau-r)E^{[m]}_{\{\mathrm{CAB}\}}(r)E^{[m-1]}_{\{\mathrm{BCA}\}}(\tau-r)E^{[m]}_{\{\mathrm{BCA}\}}(r)]\rho_{\mathrm{sys}}^{ABC}(t_0),$$

where we denote an application of the triple-shifted periodic boundary conditions to the tensor network $X$ as $\mathcal{P}_3(X)$. The contraction cost is $O(m\chi^7 d^8)$.

The generalization to larger number of the nodes $n$ $(A_1,A_2,\ldots,A_n)$ in the setup, thus, requires the following steps. First, one needs to construct $n$ 1D cascaded chains. The unit cell of each chain is obtained using the cyclic permutation of the node order $(A_1,A_2,\ldots,A_n)$. The second step requires calculating the total propagators for each chain with two-site superoperators, which are different for each chain as long as the nodes in the setup are not identical. This is followed by the contraction of the resulting $n$ propagators with the periodic boundary conditions shifted by $n$ sites and applying the whole structure to the initial density matrix of the nodes. One can write a generalized expression for the system density matrix of $n$ nodes at time $t_n$ as

$$\rho_{\mathrm{sys}}^{\{A_1,A_2,\ldots,A_n\}}(t_n)=\mathcal{P}_n[E^{[m]}_{\{A_1,A_2,\ldots,A_n\}}(\tau-r,r)E^{[m]}_{\{A_n,A_1,\ldots,A_{n-1}\}}(\tau-r,r)\ldots E^{[m]}_{\{A_2,A_3,\ldots,A_1\}}(\tau-r,r)]\rho_{\mathrm{sys}}^{\{A_1,A_2,\ldots,A_n\}}(t_0),$$

where we use the shorthand notation $E^{[m]}(\tau-r,r)\equiv E^{[m-1]}(\tau-r)E^{[m]}(r)$. While the chain evolution can be performed in parallel, the cost of the propagators' contraction scales exponentially with the number of nodes $O(m\chi^{3+2(n-1)}d^{4+2(n-1)})$.

### 2. General multinode setups

In this appendix, we provide a recipe on how our method can be used for generalized setups with coherent feedback loops. Specifically, multinode setups with nodes coupled to a bidirectional waveguide with unequal distances between the nodes and, therefore, unequal delay times of the excitation propagation. Below, we discuss two examples that illustrate the important points of the method generalization: (i) a setup with two atoms and a mirror and (ii) three atoms coupled to a bidirectional waveguide.

Let us demonstrate how to apply the algorithm to a setup with two driven atoms $A$ and $B$ connected to a bidirectional waveguide terminated by a mirror. The delay time between nodes $A$ and $B$ and between node $B$ and the mirror is $\tau=2x/v$, and the characteristic round-trip phase is $\phi=-\omega_0\tau$ [see Fig. 17(a)]. The interaction Hamiltonian in the frame rotating with the laser frequency $\omega_0$ and in the interaction picture with respect to the bath Hamiltonian for this setup reads

$$H_{\mathrm{int}}(t)=\mathrm{i}\hbar\left[\sqrt{\gamma_R^B}b^\dagger(t+2\tau)e^{\mathrm{i}\phi}c_R^B+\sqrt{\gamma_L^B}b^\dagger(t+\tau)e^{\mathrm{i}(2\phi+\pi)}c_L^B+\sqrt{\gamma_R^A}b^\dagger(t+3\tau)c_R^A+\sqrt{\gamma_L^A}b^\dagger(t)e^{\mathrm{i}(3\phi+\pi)}c_L^A-\mathrm{H.c.}\right]. \tag{D8}$$

We note here that this setup can be considered as a setup with atom $A$ connected to feedback loop with a processing node (atom $B$) inside (cf. Fig. 1). We build a tensor network representing the total wave function $|\Psi(t)\rangle$ of both nodes and the state of the waveguide and then obtain the tensor network for the reduced density matrix $\rho_{\rm sys}(t) = {\rm tr}_{\mathcal{H}_B}\{|\Psi(t)\rangle\langle\Psi(t)|\}$. The size of this network is $k \times 2m$, where $k$ is a round-trip time $\tau$ in units of $\Delta t$ and $m = \lceil n/k \rceil$, i.e., total evolution time $t_n - t_0$ in units of the time $\tau$, rounded up. The transfer operator for this network is the propagator describing the evolution of a generalized 1D cascaded chain. The chain consists of replicas of nodes $A$ and $B$ ($ABABAB\ldots$) at times $\{0, \tau, 2\tau, 3\tau, \ldots\}$ resulting in a total number of sites being $2m$ [see Fig. 17(a)]. The corresponding propagator for this chain satisfies the following equations:

$$\frac{d}{ds}E^{[2m]}(s) = \mathcal{L}^{[2m]}E^{[2m]}(s), \tag{D9}$$

with the Lindblad superoperators defined as

$$\mathcal{L}^{[2m]} = \sum_{j\in{\rm odd}} \mathcal{L}^{\rm casc}_{j,(4)} + \mathcal{L}^{\rm boundary}, \tag{D10}$$

where the summation goes over odd $j$ from 1 to $2m-7$ and $\mathcal{L}^{\rm casc}_{j,(4)}$ describes a four-node cascaded interaction [indicated by the subscript (4)] from replica $A$ at position $j$ through replicas $B$ at positions $j+3$ and $j+5$ to replica $A$ at position $j+6$:

$$\mathcal{L}^{\rm casc}_{j,(4)}X = -\mathbb{i}[H^{\rm casc}_{j,(4)}, X] + \sum_{p>k}\mathcal{D}[R_p + L_k]X, \tag{D11}$$

with the cascaded Hamiltonian

$$H^{\rm casc}_{j,(4)} = \frac{1}{2}\left(\sum_k H_{{\rm sys},k} + \sum_{p>k}\mathbb{i}(R_k^\dagger L_p - L_p^\dagger R_k)\right),$$

where the summation $p, k$ goes over the set $S = \{j, j+3, j+5, j+6\}$. Boundary terms now include three-node cascaded interactions $A \to B \to B$ and $B \to B \to A$ and two-node cascaded interactions $A \to B$ and $B \to A$:

$$\begin{aligned}\mathcal{L}^{{\rm bd}L}X &= \mathcal{L}_1^{{\rm bd}L}X + \mathcal{D}[L_1]X + \mathcal{L}^{\rm cascL}_{2,(3)}X + \mathcal{L}^{\rm cascL}_{2,(2)}X,\\ \mathcal{L}^{{\rm bd}R}X &= \mathcal{L}_{2m}^{{\rm bd}R}X + \mathcal{D}[R_{2m}]X + \mathcal{L}^{\rm cascR}_{2m-5,(3)}X + \mathcal{L}^{\rm cascR}_{2m-3,(2)}X,\end{aligned} \tag{D12}$$

where operators $\mathcal{L}_1^{{\rm bd}L}$ and $\mathcal{L}_{2m}^{{\rm bd}R}$ are analogous to Eq. (18). Cascaded Lindblad operators $\mathcal{L}^{\rm cascL}_{i,(3)}$ and $\mathcal{L}^{\rm cascL}_{i,(2)}$ are analogous to Eq. (D10) with the summation going over sets $\{i, i+2, i+3\}$ and $\{i, i+2\}$ correspondingly and for $\mathcal{L}^{\rm cascR}_{i,(3)}$ and $\mathcal{L}^{\rm cascR}_{i,(2)}$ with sets $\{i, i+3, i+5\}$ and $\{i, i+3\}$ correspondingly. To calculate the reduced density matrix of the nodes $A$ and $B$ at time $t_n$, we calculate the total propagator for the chain, contract it with double-shifted periodic boundary conditions, and then apply the result to the initial density matrix [see Figs. 17(b) and 17(c)]:

$$\rho^{AB}_{\rm sys}(t_n) = \mathcal{P}_2[E^{[2m-2]}(\tau - r)E^{[2m]}(r)]\rho^{AB}_{\rm sys}(t_0), \tag{D13}$$

where we use $\mathcal{P}_2(X)$ to denote an application of the double-shifted periodic boundary conditions to the tensor network $X$. The cost of the total contraction in Eq. (D13) is $O(2m\chi^3 d^6)$.

The results of the numerical representation of the above procedure are presented in Fig. 18. Specifically, Fig. 18(a) shows an area law of entanglement entropy with the number of round-trip times corresponding to the number of $A$ or $B$ nodes in the chain $m$. The dynamics of the nodes is shown in Fig. 18(b), where we plot the excitation probability of both atoms as a function time.

We now generalize our method for a setup with three nodes ($A$, $B$, and $C$) coupled to a waveguide with delay times $\tau_{AB} = \alpha\tau$ and $\tau_{BC} = \beta\tau$, where $\tau = x/v$ is a characteristic delay time, and phases $\phi_{AB} = -\omega_0\tau_{AB}$ and $\phi_{BC} = -\omega_0\tau_{BC}$ acquired by the photons after propagating between the corresponding nodes [see Fig. 17(d)]. The interaction Hamiltonian in the frame rotating with the laser frequency $\omega_0$ and in the interaction picture with respect to the bath Hamiltonian for this setup reads

$$\begin{aligned}H_{\rm int}(t) = \mathbb{i}\hbar\Big[&\sqrt{\gamma_R^C}b^\dagger(t + [\alpha+\beta]\tau)e^{\mathbb{i}(\phi_{AB}+\phi_{BC})}c_R^C + \sqrt{\gamma_L^C}b^\dagger(t)c_L^C + \sqrt{\gamma_R^B}b^\dagger(t+\alpha\tau)e^{\mathbb{i}\phi_{AB}}C_R^B\\ &+ \sqrt{\gamma_L^B}b^\dagger(t+\beta\tau)e^{\mathbb{i}\phi_{BC}}c_L^B + \sqrt{\gamma_R^A}b^\dagger(t)c_R^A + \sqrt{\gamma_L^A}b^\dagger(t+[\alpha+\beta]\tau)e^{\mathbb{i}(\phi_{AB}+\phi_{BC})}c_L^A - {\rm H.c.}\Big].\end{aligned} \tag{D14}$$

We note here that the characteristic delay time $\tau$ can be as small as $\Delta t$, allowing one to work with setups with arbitrary delay times between the nodes. The tensor network of the reduced density matrix of the nodes has a transfer operator equivalent to a propagator of a generalized cascaded chain shown in Fig. 17(d). This chain consists of $3m$ replicas of nodes $A$, $B$, and $C$, where $m = \lceil (t_n - t_0)/\tau \rceil$. There are two types of cascaded interactions: between the nodes $A \to B \to C$ at positions $\{i, i+3\alpha+1, i+(\alpha+\beta)+2\}$ with $i = 3n_i + 1, n_i \in \{0, 1, 2, 3, \ldots\}$ and between the nodes $C \to B \to A$ at positions $\{i+2, i+3\beta+1, i+3(\alpha+\beta)\}$ [cf. Fig. 17(d)]. As before, we obtain the total

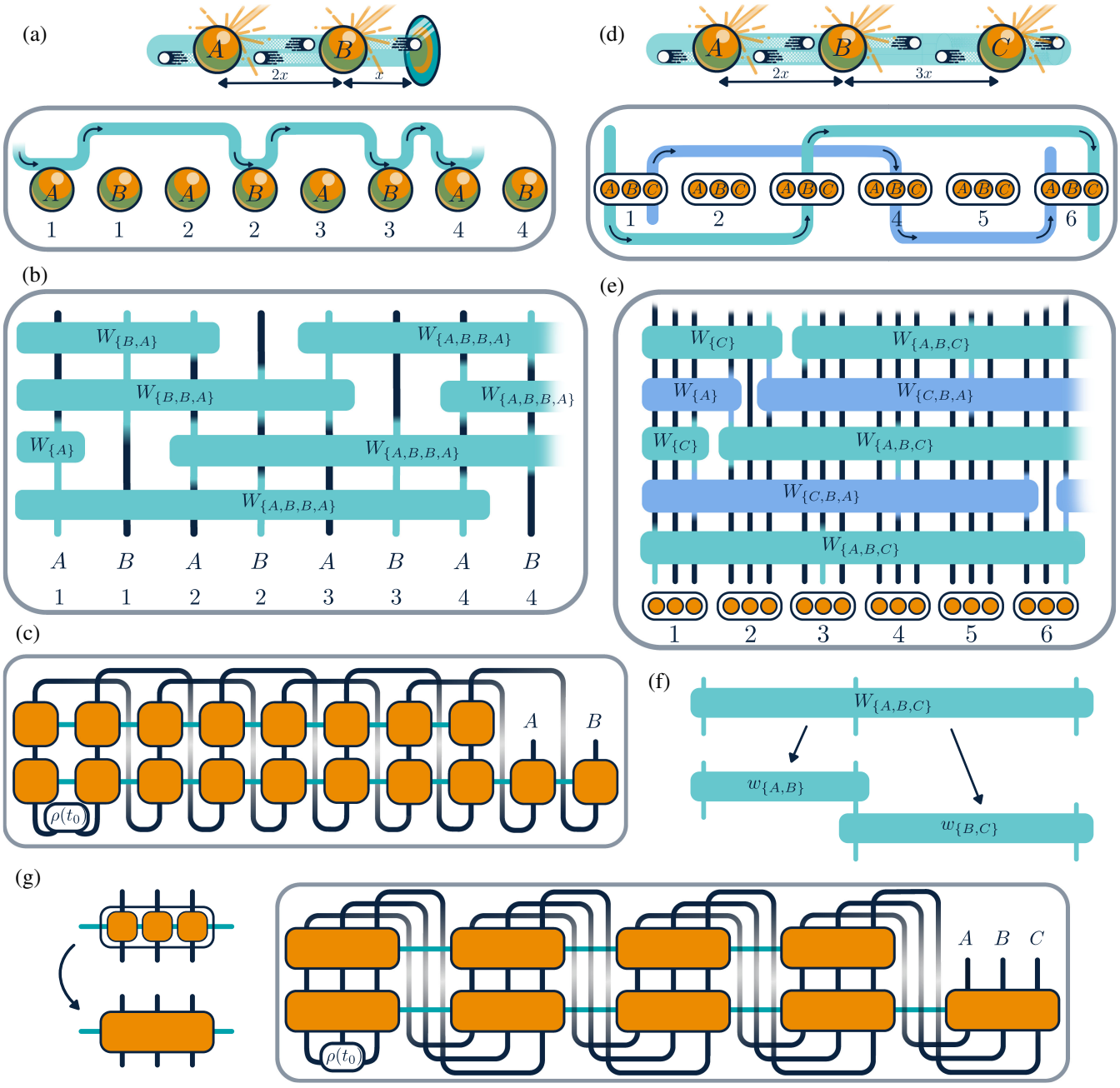


FIG. 17. General multinode setups. (a) Two atoms in front of the mirror Eq. (D8) are mapped to a generalized 1D cascaded chain of systems' replicas $A$ and $B$ at different times. This cascaded chain has one type of cascaded interaction indicated by the light blue line going through the replicas $\{A, B, B, A\}$. The interaction occurs between each replicas $\{A, B, B, A\}$ in the right order as indicated in the text [see Eq. (D10)]. (b) The evolution operators $W_{A,B,B,A}$, $W_{A,B,B}$, $W_{A,B,B}$, etc., generated by the Lindblad operators Eqs. (D11) and (D12) are applied to the initial identity operator of the chain using the TEBD method. (c) The propagators obtained through the evolution are then contracted with the double-shifted periodic boundary conditions and applied to the initial density operator as in Eq. (D13). (d) Setup with three atoms connected to a bidirectional waveguide with unequal delay times Eq. (D14) is mapped to a generalized 1D cascaded chain consisting of replicas $A$, $B$, and $C$ at different times with two types of cascaded interactions between $A$, $B$, $C$ and $C$, $B$, $A$ indicated by blue lines. (e) The propagator is obtained after the MPS evolution of this chain with the evolution operators $W_{A,B,C}$, $W_{C,B,A}$, etc., generated by the corresponding cascaded Lindblad operators. (f) To apply a multisite evolution operator, we break it down in multiple two-site operators and apply them one after another. (g) The propagators in MPS form are then contracted with the triple-shifted periodic boundary conditions, where we for simplicity depict three tensors corresponding to $A$, $B$, and $C$ at the same time period as a single larger block.

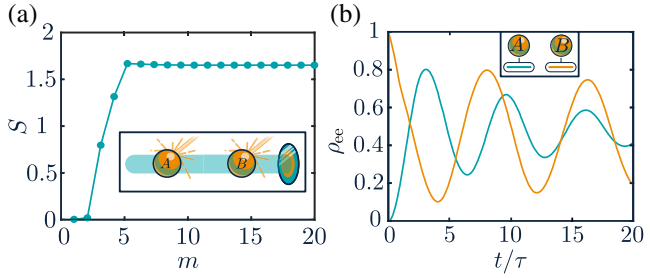


FIG. 18. Setup with two driven atoms in front of a mirror [Fig. 17(a)]. (a) Dependence of the bipartite entropy $S$ on the length of the chain $m$ exhibiting an area law. Note that for each site $m$ we indeed have two atoms $A$ and $B$ at time $m\Delta\tau$ (b) $\rho_{ee}^{A}$ and $\rho_{ee}^{B}$ of the two atoms $A$ and $B$ as a function of $t/\tau$. Atom $A$ is initially in the ground state and atom $B$ in the excited. For both plots, the parameters are $\gamma_L^A = \gamma_R^A = \gamma_L^B = \gamma_R^B = \Gamma/2$, $\Omega_A = 5\Gamma$, $\Omega_B = 4\Gamma$, $\phi = 0$, $\Gamma\tau = 0.2$, and $\chi = 120$.

propagator of the chain for time $\tau$ by applying the evolution operators of the Lindblad master equation, $W_{A,B,C}$ and $W_{C,B,A}$ as well as boundary terms, to the identity operator as shown in Fig. 17(e). To obtain the density matrix of the nodes, we contract the resulting matrix product operator using triple-shifted periodic boundary conditions and apply it to the initial density matrix as demonstrated in Figs. 17(g)–17(k). The cost of this contraction is $O(3m\chi^3 d^8)$.

As discussed above, we consider a setup with $\alpha = 2$ and $\beta = 3$ and calculate the entropy of the total propagator and the resulting density matrix of three nodes. The results are presented in Fig. 19. We again observe an area law for the entanglement entropy as can be seen from Fig. 19(a). The excitation probability dependence on time is shown in Fig. 19(b).

During the evolution of the matrix product operator for both types of setups discussed above, we separate for simplicity the multisite evolution operator into a number of two-site operators as shown in Fig. 17(f). Then we apply

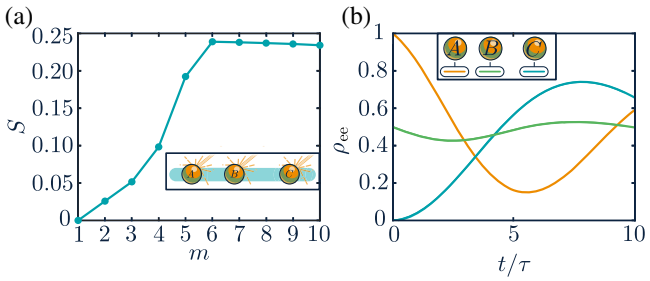


FIG. 19. Setup with three driven atoms coupled to a bidirectional waveguide [Fig. 17(d)]. (a) Dependence of the bipartite entropy $S$ on the length of the chain $m$ exhibiting an area law. Note that for each site $m$ we have three atoms $A$, $B$, and $C$ at time $m\Delta\tau$ (b) $\rho_{ee}^{A}$, $\rho_{ee}^{B}$, and $\rho_{ee}^{C}$ as a function of $t/\tau$. Atom $A$ is initially in the excited state, atom $C$ in the ground state, and atom $B$ in a symmetric superposition. For both plots, the parameters are $\gamma_A = \gamma_B = \gamma_C = \Gamma/2$, $\Omega_A = 5\Gamma$, $\Omega_B = 6\Gamma$, $\Omega_B = 4\Gamma$, $\phi_{AB} = \phi_{BC} = 0$, $\Gamma\tau = 0.1$, $\Gamma\tau_{AB} = 0.2$, $\Gamma\tau_{BC} = 0.3$, and $\chi = 120$.

SWAP operators to move the two sites of interest close to each other and perform a step of TEBD algorithm by applying the two-site operator. After that, another series of SWAP operators is applied to return to the original order of the chain. These additional steps in comparison to the algorithms presented in the main text, of course, increase the cost of propagator evolution. Specifically, the cost grows linearly with the number of nodes participating in cascaded interaction and with the value $k_{\max} = \tau_{\max}/\tau$, that is, the maximum delay time in the setup in units of characteristic time $\tau$.

We note here that the effective dimension of the bosonic modes associated to each time bin of left- (right-) propagating modes for the multinode setups is $\dim(\mathcal{H}_i) = 2$ as for the case of the atom in front of the mirror. Again, the probability to have more than one excitation $n_e$ in a single time bin is proportional to $(\Delta t)^{n_e}$. As mentioned before, all our results are converged in $\Delta t$; that is, we choose such $\Delta t$ that computational errors of the order of $\Delta t^2$ and higher are negligible.

## APPENDIX E: RUN-TIME BENCHMARKING

In this appendix, we present a quantitative comparison of the runtime of the algorithm presented in this paper and the algorithm proposed in Ref. [41] on the same problem. Specifically, we compare the computational time required to reach the state of the driven atom in front of the mirror with a fidelity $F \geq 0.9999$ for both methods. This is done by first calculating the (numerically) the exact solution using the new method with a large bond dimension (and a rigorous convergence check); then, for each data point, we calculate the state of the atom for both methods for some fixed, finite bond dimension and check the fidelity with the exact solution. If the fidelity is below the required precision, the bond dimension is increased until the precision limit is met. The computational time is measured only for the value of bond dimension that corresponds to the required fidelity. The results presented in Fig. 20 show the dependence of these computational times on the delay time for two different Rabi frequencies. For the parameters chosen in this figure, one finds a decrease of the run-time for our new method in comparison with the method in Ref. [41] of up to 3 orders of magnitude. In addition, the favorable scaling with time delay is clearly visible. Furthermore, we show the dynamics calculated with the method in Ref. [41] and the method proposed in our manuscript with the fixed bond dimension $\chi = 15$ for both methods in Fig. 20(c) and compare it with the exact solution. One can see that, while the new method reproduces exact dynamics well even with this small bond dimension, the method in Ref. [41] struggles to converge. Moreover, as indicated in the right side of the plot, the new method requires 2 orders of magnitude less time to calculate the dynamics presented in the plot than the method in Ref. [41]. We also note here that, while the method in Ref. [41] allows one to reach the steady state of the atom for

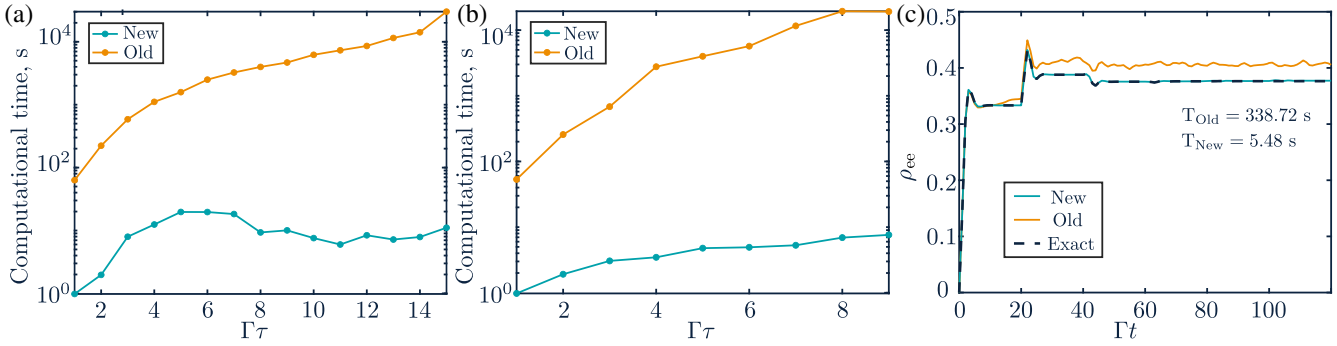


FIG. 20. Computational time dependence on delay time for the method in Ref. [41] (old) and the method of our manuscript (new). Driving strengths are (a) $\Omega = 0.2\Gamma$, (b) $\Omega = \Gamma$, for both plots $\phi = \pi$, $\Delta/\Gamma = 0$, and the Trotter step is $\Gamma\Delta t = 0.005$. (c) Excited state probability dynamics calculated using the method in Ref. [41] (old) and our method (new) with the computational time indicated on the right side. The bond dimension $\chi = 15$ for both methods.

some finite $\tau$, it can be done only indirectly through a long-time evolution (see also Table I). Contrary to that, the new method can target the steady state directly and for any delay time, which to our knowledge was not possible before.

### 1. Approach based on Laplace transform

Finally, we consider an analytical approach based on the Laplace transform that is often used in Markovian systems to study the steady state and discuss the issues that arise when this is applied to the current problems. First, we discuss this method in the absence of a driving field, where it works, and then highlight the difference and difficulties that are encountered when the driving field is included. For this, we first explicitly write down the dynamical equation for the system operator $c(t)$, whose evolution is governed by the Hamiltonian in Eq. (6) with zero driving:

$$\dot{c}(t) = \mathbb{i}\Delta c(t) - \gamma c(t) + \gamma e^{-\mathbb{i}\phi} c(t-\tau) + \sqrt{\gamma}\sigma_z(t) b(t+\tau) + \sqrt{\gamma} e^{-\mathbb{i}\phi}\sigma_z(t) b(t), \tag{E1}$$

where, for simplicity, we set $c_R(t) = c_L(t) = c(t)$ and $\gamma_R = \gamma_L = \gamma$. After performing Laplace transform of the equation above and applying it to the initial state of the setup at time $t = 0$, we obtain

$$\tilde{c}(s)|\Psi(0)\rangle = -\frac{\gamma e^{-\mathbb{i}\phi-\tau s}\tilde{c}(s)|\Psi(0)\rangle}{s+\gamma-\mathbb{i}\Delta} + c(0^-)|\Psi(0)\rangle. \tag{E2}$$

This equation can be integrated analytically, giving us

$$c(t)|\Psi(0)\rangle = c(0)|\Psi(0)\rangle e^{-(\gamma-\mathbb{i}\Delta)t} \times \sum_{p=0}^{\lfloor t/\tau\rfloor} \frac{1}{p!}\left[-\gamma e^{-\mathbb{i}\phi+(\gamma-\mathbb{i}\Delta)\tau}(t-p\tau)\right]^p. \tag{E3}$$

Equation (E2) is easy to analyze using the final-value theorem to find the steady state, that is,

$$\lim_{s\to 0} s\tilde{c}(s)|\Psi(0)\rangle = \lim_{s\to 0}\frac{sc(0)|\Psi(0)\rangle}{s-\mathbb{i}\Delta+\gamma(1+e^{-\mathbb{i}\phi-\tau s})},$$
$$\lim_{s\to 0} s\tilde{c}(s)|\Psi(0)\rangle \to \begin{cases} \frac{c(0)|\Psi(0)\rangle}{1+\gamma\tau}, & \text{if } \mathbb{i}\Delta-\gamma(1+e^{-\mathbb{i}\phi}) = 0, \\ 0, & \text{otherwise.} \end{cases} \tag{E4}$$

When the driving is switched on, Eq. (E1) has to be generalized as

$$\dot{c}(t) = \mathbb{i}\Delta c(t) + \frac{\mathbb{i}\Omega}{2}\sigma_z(t) - \gamma c(t) + \gamma e^{-\mathbb{i}\phi}\sigma_z(t)c(t-\tau) + \sqrt{\gamma}\sigma_z(t)b(t+\tau) + \sqrt{\gamma}e^{-\mathbb{i}\phi}\sigma_z(t)b(t). \tag{E5}$$

In the same fashion, one obtains

$$\dot{\sigma}_z(t) = \mathbb{i}\Omega[c^\dagger(t) - c(t)] - 4\gamma c^\dagger(t)c(t) - 2\sqrt{\gamma}c^\dagger(t)[\sqrt{\gamma}e^{-\mathbb{i}\phi}c(t-\tau) + b(t+\tau) + e^{-\mathbb{i}\phi}b(t)] - 2[\gamma e^{\mathbb{i}\phi}c^\dagger(t-\tau) + \sqrt{\gamma}b^\dagger(t+\tau) + \sqrt{\gamma}e^{\mathbb{i}\phi}b^\dagger(t)]c(t). \tag{E6}$$

This is a nonlinear system of equations for the system operators. After applying the first equation above to the initial wave function at time $t = 0$ and performing Laplace transform, we arrive at

$$[\tilde{c}(s) - c(0^-)]|\Psi(0)\rangle = \frac{1}{s+\gamma-\mathbb{i}\Delta}\left[\mathbb{i}\frac{\Omega}{2}\tilde{\sigma}_z(s)|\Psi(0)\rangle + \frac{\gamma e^{-\mathbb{i}\phi}}{2\pi\mathbb{i}}\lim_{T\to\infty}\int_{a-\mathbb{i}T}^{a+\mathbb{i}T}\tilde{\sigma}_z(s')\tilde{c}(s-s')|\Psi(0)\rangle e^{-\tau(s-s')}ds'\right], \tag{E7}$$

where the integral is taken along the line $\mathrm{Re}(s) = a$ chosen in such way that it lies within the region of convergence of $\tilde{c}(s)$. In its general form, this equation is nonlinear and has an integral that requires a knowledge of $\tilde{\sigma}_z(s')\tilde{c}(s-s')|\Psi(0)\rangle$ for various $s'$. To calculate the steady-state excitation probability, one could again use the final-value theorem and consider the limit $s \to 0$. Unfortunately, even in this limit the aforementioned integral is not simplified, and to the best of our knowledge the steady state can, thus, not be obtained from this expression.


[1] H. M. Wiseman and G. J. Milburn, *Quantum theory of optical feedback via homodyne detection*, Phys. Rev. Lett. **70**, 548 (1993).

[2] H. M. Wiseman, *Quantum theory of continuous feedback*, Phys. Rev. A **49**, 2133 (1994).

[3] H. M. Wiseman and G. J. Milburn, *Quantum Measurement and Control* (Cambridge University Press, Cambridge, England, 2010).

[4] A. C. Doherty, S. Habib, K. Jacobs, H. Mabuchi, and S. M. Tan, *Quantum feedback control and classical control theory*, Phys. Rev. A **62**, 012105 (2000).

[5] J. Zhang, Y.-x. Liu, R.-B. Wu, K. Jacobs, and F. Nori, *Quantum feedback: Theory, experiments, and applications*, Phys. Rep. Quantum Feedback **679**, 1 (2017).

[6] A. Kubanek, M. Koch, C. Sames, A. Ourjoumtsev, P. W. H. Pinkse, K. Murr, and G. Rempe, *Photon-by-photon feedback control of a single-atom trajectory*, Nature (London) **462**, 898 (2009).

[7] C. Sayrin, I. Dotsenko, X. Zhou, B. Peaudecerf, T. Rybarczyk, S. Gleyzes, P. Rouchon, M. Mirrahimi, H. Amini, M. Brune, J.-M. Raimond, and S. Haroche, *Real-time quantum feedback prepares and stabilizes photon number states*, Nature (London) **477**, 73 (2011).

[8] R. Vijay, C. Macklin, D. H. Slichter, S. J. Weber, K. W. Murch, R. Naik, A. N. Korotkov, and I. Siddiqi, *Stabilizing Rabi oscillations in a superconducting qubit using quantum feedback*, Nature (London) **490**, 77 (2012).

[9] M. Hirose and P. Cappellaro, *Coherent feedback control of a single qubit in diamond*, Nature (London) **532**, 77 (2016).

[10] L. Magrini, P. Rosenzweig, C. Bach, A. Deutschmann-Olek, S. G. Hofer, S. Hong, N. Kiesel, A. Kugi, and M. Aspelmeyer, *Real-time optimal quantum control of mechanical motion at room temperature*, Nature (London) **595**, 373 (2021).

[11] S. Lloyd, *Coherent quantum feedback*, Phys. Rev. A **62**, 022108 (2000).

[12] K. Jacobs, X. Wang, and H. M. Wiseman, *Coherent feedback that beats all measurement-based feedback protocols*, New J. Phys. **16**, 073036 (2014).

[13] C. W. Gardiner and M. J. Collett, *Input and output in damped quantum systems: Quantum stochastic differential equations and the master equation*, Phys. Rev. A **31**, 3761 (1985).

[14] I. C. Hoi, A. F. Kockum, L. Tornberg, A. Pourkabirian, G. Johansson, P. Delsing, and C. M. Wilson, *Probing the quantum vacuum with an artificial atom in front of a mirror*, Nat. Phys. **11**, 1045 (2015).

[15] X. Gu, A. F. Kockum, A. Miranowicz, Y. xi Liu, and F. Nori, *Microwave photonics with superconducting quantum circuits*, Phys. Rep. **718–719**, 1 (2017).

[16] H. Pichler, S. Choi, P. Zoller, and M. D. Lukin, *Universal photonic quantum computation via time-delayed feedback*, Proc. Natl. Acad. Sci. U.S.A. **114**, 11362 (2017).

[17] Y. Yu, F. Ma, X.-Y. Luo, B. Jing, P.-F. Sun, R.-Z. Fang, C.-W. Yang, H. Liu, M.-Y. Zheng, X.-P. Xie, W.-J. Zhang, L.-X. You, Z. Wang, T.-Y. Chen, Q. Zhang, X.-H. Bao, and J.-W. Pan, *Entanglement of two quantum memories via fibres over dozens of kilometres*, Nature (London) **578**, 240 (2020).

[18] D. Lago-Rivera, S. Grandi, J. V. Rakonjac, A. Seri, and H. de Riedmatten, *Telecom-heralded entanglement between multimode solid-state quantum memories*, Nature (London) **594**, 37 (2021).

[19] T. van Leent, M. Bock, F. Fertig, R. Garthoff, S. Eppelt, Y. Zhou, P. Malik, M. Seubert, T. Bauer, W. Rosenfeld, W. Zhang, C. Becher, and H. Weinfurter, *Entangling single atoms over 33 km telecom fibre*, Nature (London) **607**, 69 (2022).

[20] P. Campagne-Ibarcq, E. Zalys-Geller, A. Narla, S. Shankar, P. Reinhold, L. Burkhart, C. Axline, W. Pfaff, L. Frunzio, R. J. Schoelkopf, and M. H. Devoret, *Deterministic remote entanglement of superconducting circuits through microwave two-photon transitions*, Phys. Rev. Lett. **120**, 200501 (2018).

[21] Y. P. Zhong, H.-S. Chang, K. J. Satzinger, M.-H. Chou, A. Bienfait, C. R. Conner, É. Dumur, J. Grebel, G. A. Peairs, R. G. Povey, D. I. Schuster, and A. N. Cleland, *Violating Bell's inequality with remotely connected superconducting qubits*, Nat. Phys. **15**, 741 (2019).

[22] C. Eichler, J. Mlynek, J. Butscher, P. Kurpiers, K. Hammerer, T. J. Osborne, and A. Wallraff, *Exploring interacting quantum many-body systems by experimentally creating continuous matrix product states in superconducting circuits*, Phys. Rev. X **5**, 041044 (2015).

[23] C. J. Axline, L. D. Burkhart, W. Pfaff, M. Zhang, K. Chou, P. Campagne-Ibarcq, P. Reinhold, L. Frunzio, S. M. Girvin, L. Jiang, M. H. Devoret, and R. J. Schoelkopf, *On-demand quantum state transfer and entanglement between remote microwave cavity memories*, Nat. Phys. **14**, 705 (2018).

[24] V. Krutyanskiy, M. Canteri, M. Meraner, V. Krcmarsky, and B. P. Lanyon, *Multimode ion-photon entanglement over 101 kilometers of optical fiber*, arXiv:2308.08891.

[25] V. S. Ferreira, J. Banker, A. Sipahigil, M. H. Matheny, A. J. Keller, E. Kim, M. Mirhosseini, and O. Painter, *Collapse and revival of an artificial atom coupled to a structured photonic reservoir*, Phys. Rev. X **11**, 041043 (2021).

[26] S. Chakram, K. He, A. V. Dixit, A. E. Oriani, R. K. Naik, N. Leung, H. Kwon, W.-L. Ma, L. Jiang, and D. I. Schuster, *Multimode photon blockade*, Nat. Phys. **18**, 879 (2022).

[27] G. Andersson, B. Suri, L. Guo, T. Aref, and P. Delsing, *Non-exponential decay of a giant artificial atom*, Nat. Phys. **15**, 1123 (2019).

[28] A. Bienfait, K. J. Satzinger, Y. P. Zhong, H.-S. Chang, M.-H. Chou, C. R. Conner, É. Dumur, J. Grebel, G. A. Peairs, R. G. Povey, and A. N. Cleland, *Phonon-mediated*

*quantum state transfer and remote qubit entanglement*, Science **364**, 368 (2019).

[29] É. Dumur, K. J. Satzinger, G. A. Peairs, M.-H. Chou, A. Bienfait, H.-S. Chang, C. R. Conner, J. Grebel, R. G. Povey, Y. P. Zhong, and A. N. Cleland, *Quantum communication with itinerant surface acoustic wave phonons*, npj Quantum Inf. **7**, 173 (2021).

[30] M. Kraft, S. M. Hein, J. Lehnert, E. Schöll, S. Hughes, and A. Knorr, *Time-delayed quantum coherent pyragas feedback control of photon squeezing in a degenerate parametric oscillator*, Phys. Rev. A **94**, 023806 (2016).

[31] N. Német and S. Parkins, *Enhanced optical squeezing from a degenerate parametric amplifier via time-delayed coherent feedback*, Phys. Rev. A **94**, 023809 (2016).

[32] J. E. Gough, R. Gohm, and M. Yanagisawa, *Linear quantum feedback networks*, Phys. Rev. A **78**, 062104 (2008).

[33] M. Laakso and M. Pletyukhov, *Scattering of two photons from two distant qubits: Exact solution*, Phys. Rev. Lett. **113**, 183601 (2014).

[34] Yao-Lung L. Fang and H. U. Baranger, *Waveguide QED: Power spectra and correlations of two photons scattered off multiple distant qubits and a mirror*, Phys. Rev. A **91**, 053845 (2015).

[35] K. Sinha, P. Meystre, E. A. Goldschmidt, F. K. Fatemi, S. L. Rolston, and P. Solano, *Non-Markovian collective emission from macroscopically separated emitters*, Phys. Rev. Lett. **124**, 043603 (2020).

[36] Q. Y. Cai and W. Z. Jia, *Coherent single-photon scattering spectra for a giant-atom waveguide-QED system beyond the dipole approximation*, Phys. Rev. A **104**, 033710 (2021).

[37] K. Barkemeyer, A. Knorr, and A. Carmele, *Heisenberg treatment of multiphoton pulses in waveguide QED with time-delayed feedback*, Phys. Rev. A **106**, 023708 (2022).

[38] G. Calajó, Yao-Lung L. Fang, H. U. Baranger, and F. Ciccarello, *Exciting a bound state in the continuum through multiphoton scattering plus delayed quantum feedback*, Phys. Rev. Lett. **122**, 073601 (2019).

[39] V. Giovannetti, P. Tombesi, and D. Vitali, *Non-Markovian quantum feedback from homodyne measurements: The effect of a nonzero feedback delay time*, Phys. Rev. A **60**, 1549 (1999).

[40] F. Dinc, *Diagrammatic approach for analytical non-Markovian time evolution: Fermi's two-atom problem and causality in waveguide quantum electrodynamics*, Phys. Rev. A **102**, 013727 (2020).

[41] H. Pichler and P. Zoller, *Photonic circuits with time delays and quantum feedback*, Phys. Rev. Lett. **116**, 093601 (2016).

[42] A. L. Grimsmo, *Time-delayed quantum feedback control*, Phys. Rev. Lett. **115**, 060402 (2015).

[43] P. O. Guimond, M. Pletyukhov, H. Pichler, and P. Zoller, *Delayed coherent quantum feedback from a scattering theory and a matrix product state perspective*, Quantum Sci. Technol. **2**, 044012 (2017).

[44] T. Ramos, B. Vermersch, P. Hauke, H. Pichler, and P. Zoller, *Non-Markovian dynamics in chiral quantum networks with spins and photons*, Phys. Rev. A **93**, 062104 (2016).

[45] A. Ask and G. Johansson, *Non-Markovian steady states of a driven two-level system*, Phys. Rev. Lett. **128**, 083603 (2022).

[46] S. J. Whalen, A. L. Grimsmo, and H. J. Carmichael, *Open quantum systems with delayed coherent feedback*, Quantum Sci. Technol. **2**, 044008 (2017).

[47] S. Campbell, F. Ciccarello, G. M. Palma, and B. Vacchini, *System-environment correlations and Markovian embedding of quantum non-Markovian dynamics*, Phys. Rev. A **98**, 012142 (2018).

[48] G. Crowder, H. Carmichael, and S. Hughes, *Quantum trajectory theory of few-photon cavity-QED systems with a time-delayed coherent feedback*, Phys. Rev. A **101**, 023807 (2020).

[49] O. Kaestle, R. Finsterhoelzl, A. Knorr, and A. Carmele, *Continuous and time-discrete non-Markovian system-reservoir interactions: Dissipative coherent quantum feedback in Liouville space*, Phys. Rev. Res. **3**, 023168 (2021).

[50] X. H. H. Zhang, S. H. L. Klapp, and A. Metelmann, *Embedding of time-delayed quantum feedback in a nonreciprocal array*, arXiv:2204.02367.

[51] S. N. Filippov and I. A. Luchnikov, *Collisional open quantum dynamics with a generally correlated environment: Exact solvability in tensor networks*, Phys. Rev. A **105**, 062410 (2022).

[52] T. D. Frank, *Multivariate Markov processes for stochastic systems with delays: Application to the stochastic Gompertz model with delay*, Phys. Rev. E **66**, 011914 (2002).

[53] A. Strathearn, P. Kirton, D. Kilda, J. Keeling, and B. W. Lovett, *Efficient non-Markovian quantum dynamics using time-evolving matrix product operators*, Nat. Commun. **9**, 3322 (2018).

[54] F. A. Pollock, C. Rodríguez-Rosario, T. Frauenheim, M. Paternostro, and K. Modi, *Non-Markovian quantum processes: Complete framework and efficient characterization*, Phys. Rev. A **97**, 012127 (2018).

[55] M. R. Jørgensen and F. A. Pollock, *Exploiting the causal tensor network structure of quantum processes to efficiently simulate non-Markovian path integrals*, Phys. Rev. Lett. **123**, 240602 (2019).

[56] A. Lerose, M. Sonner, and D. A. Abanin, *Influence matrix approach to many-body Floquet dynamics*, Phys. Rev. X **11**, 021040 (2021).

[57] M. Cygorek, M. Cosacchi, A. Vagov, V. M. Axt, B. W. Lovett, J. Keeling, and E. M. Gauger, *Simulation of open quantum systems by automated compression of arbitrary environments*, Nat. Phys. **18**, 662 (2022).

[58] E. Ye and G. K.-L. Chan, *Constructing tensor network influence functionals for general quantum dynamics*, J. Chem. Phys. **155**, 0047260 (2021).

[59] Y. Liu, W. J. Munro, and J. Twamley, *A quantum ticking self-oscillator using delayed feedback*, arXiv:2307.14567.

[60] L. Guo, A. Grimsmo, A. F. Kockum, M. Pletyukhov, and G. Johansson, *Giant acoustic atom: A single quantum system with a deterministic time delay*, Phys. Rev. A **95**, 053821 (2017).

[61] C. Gardiner and P. Zoller, *The Quantum World of Ultra-Cold Atoms and Light Book II: The Physics of Quantum-Optical Devices* (Imperial College Press, London, 2015).

[62] Specifically, the time shift is chosen such that the atom interacts only with radiation modes with labels $t$ that are larger than or equal to the initial time $t_0$, i.e., $t \geq t_0$ [see Eq. (7)]. The phase choice follows the convention of Ref. [41].

[63] A. Frisk Kockum, in *Proceedings of the International Symposium on Mathematics, Quantum Theory, and Cryptography*, Mathematics for Industry, edited by T. Takagi, M. Wakayama, K. Tanaka, N. Kunihiro, K. Kimoto, and Y. Ikematsu (Springer, Singapore, 2021), pp. 125–146.
[64] F. Ciccarello, *Collision models in quantum optics*, Quantum Meas. Quantum Metrol. **4**, 53 (2017).
[65] C. W. Gardiner, *Driving a quantum system with the output field from another driven quantum system*, Phys. Rev. Lett. **70**, 2269 (1993).
[66] Modes with label $t < t_0$ never interact with the atom, and their state is irrelevant.
[67] If other initial states of the waveguide are considered, one has to appropriately generalise the expression for $V_i$ (see Appendix B).
[68] Z.-Y. Wei, D. Malz, and J. I. Cirac, *Sequential generation of projected entangled-pair states*, Phys. Rev. Lett. **128**, 010607 (2022).
[69] T. Soejima, K. Siva, N. Bultinck, S. Chatterjee, F. Pollmann, and M. P. Zaletel, *Isometric tensor network representation of string-net liquids*, Phys. Rev. B **101**, 085117 (2020).
[70] S.-H. Lin, M. P. Zaletel, and F. Pollmann, *Efficient simulation of dynamics in two-dimensional quantum spin systems with isometric tensor networks*, Phys. Rev. B **106**, 245102 (2022).
[71] L. Slattery and B. K. Clark, *Quantum circuits for two-dimensional isometric tensor networks*, arXiv:2108.02792.
[72] D. Malz and R. Trivedi, *Computational complexity of isometric tensor network states*, arXiv:2402.07975.
[73] H. J. Carmichael, *Quantum trajectory theory for cascaded open systems*, Phys. Rev. Lett. **70**, 2273 (1993).
[74] A. Soro and A. F. Kockum, *Chiral quantum optics with giant atoms*, Phys. Rev. A **105**, 023712 (2022).
[75] U. Schollwöck, *The density-matrix renormalization group in the age of matrix product states*, Ann. Phys. (Amsterdam) **326**, 96 (2011).
[76] G. Vidal, *Classical simulation of infinite-size quantum lattice systems in one spatial dimension*, Phys. Rev. Lett. **98**, 070201 (2007).
[77] In practice, following standard iTEBD algorithms, this is implemented using a two-site ansatz, $C^{[2k]}(s) = A(s)$ and $C^{[2k+1]}(s) = B(s)$ (for all $k$).
[78] F. G. S. L. Brandão, T. S. Cubitt, A. Lucia, S. Michalakis, and D. Perez-Garcia, *Area law for fixed points of rapidly mixing dissipative quantum systems*, J. Math. Phys. (N.Y.) **56**, 102202 (2015).
[79] S. Whalen, *Open quantum systems with time-delayed interactions*, Ph.D. Thesis, University of Auckland, 2015.
[80] In the proposed method, one can insert the operators after the evolution and contract multiple blocks together or insert the operations during the evolution of one block. While the first method is more demanding in terms of contraction, it requires to do evolution just once for all possible time differences between operators.
[81] For large time delays and strong driving fields, the atom can relax to a steady state within a single round-trip time. This implies that the atom is at this point no longer correlated with the photons emitted in the previous round-trip time. In the replica picture, this translates to the absence of correlation between neighboring replicas.
[82] R. Jozsa, *Fidelity for mixed quantum states*, J. Mod. Opt. **41**, 2315 (1994).
[83] B. R. Mollow, *Power spectrum of light scattered by two-level systems*, Phys. Rev. **188**, 1969 (1969).
[84] Y.-J. Liu, K. Shtengel, and F. Pollmann, *Topological quantum phase transitions in 2d isometric tensor networks*, arXiv:2312.05079.
[85] S. Barrett, K. Hammerer, S. Harrison, T. E. Northup, and T. J. Osborne, *Simulating quantum fields with cavity QED*, Phys. Rev. Lett. **110**, 090501 (2013).
[86] K. Reuer, J.-C. Besse, L. Wernli, P. Magnard, P. Kurpiers, G. J. Norris, A. Wallraff, and C. Eichler, *Realization of a universal quantum gate set for itinerant microwave photons*, Phys. Rev. X **12**, 011008 (2022).
[87] J.-C. Besse, K. Reuer, M. C. Collodo, A. Wulff, L. Wernli, A. Copetudo, D. Malz, P. Magnard, A. Akin, M. Gabureac, G. J. Norris, J. Ignacio Cirac, A. Wallraff, and C. Eichler, *Realizing a deterministic source of multipartite-entangled photonic qubits*, Nat. Commun. **11**, 4877 (2020).
[88] K. Vodenkova, *Data for the paper "Continuous Coherent Quantum Feedback with Time Delays: Tensor Network Solution", Version v1*, Zenodo (2023), https://zenodo.org/records/10143630; https://zenodo.org/records/10143651.